Consortium for Enabling Technologies and Innovation
ANNUAL WORKSHOP

Irradiation Response and Mechanical Property Changes of Conventionally and Additively Manufactured 316L Stainless Steels

Miguel Pena (Ph.D. student), Laura Hawkins (Ph.D. student), Lin Shao

Department of Nuclear Engineering
Texas A&M University

Motivation and background

AM 316: Example of the structural complexity

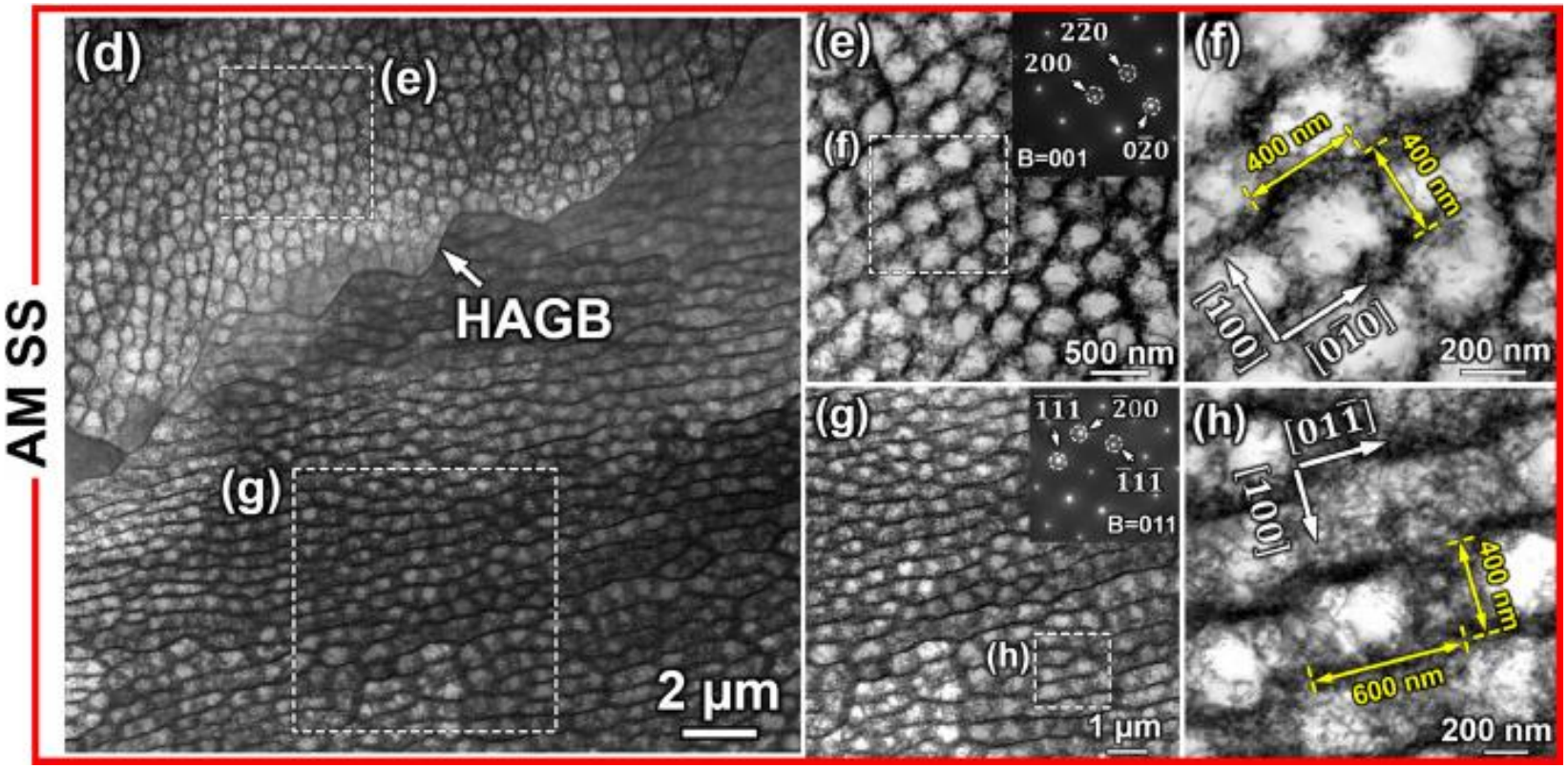

(1) Microstructure could be more important than composition.
(2) Microstructural details at resolution < 1 μm is more important than those at resolution > 1 μm.
(3) Mechanical properties and material behaviors under extremes (severe deformation, irradiation, corrosion) are important MATERIAL SIGNATURES.

Texas University Accelerator Laboratory

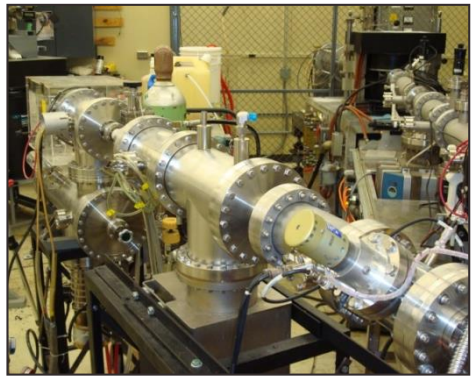

10 kV

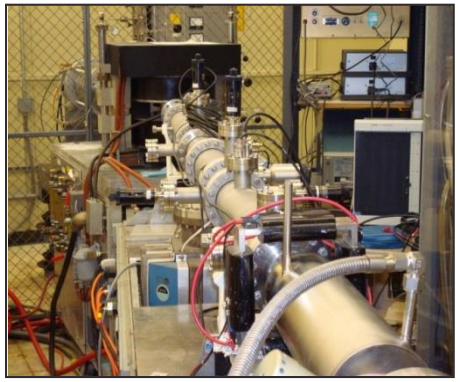

140 kV

400 kV

1.7 MV

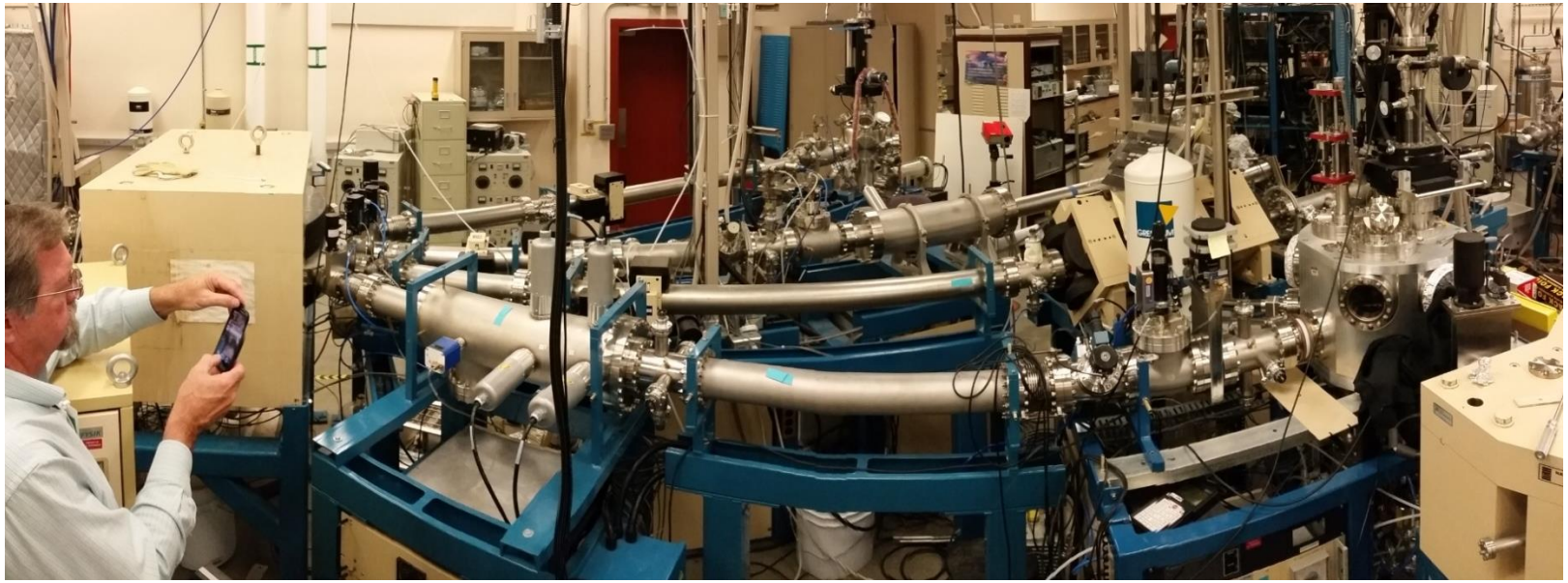

3 MV

AM 316L Pristine

Finding highlight #1: Processing-introduced pores have interface segregation.

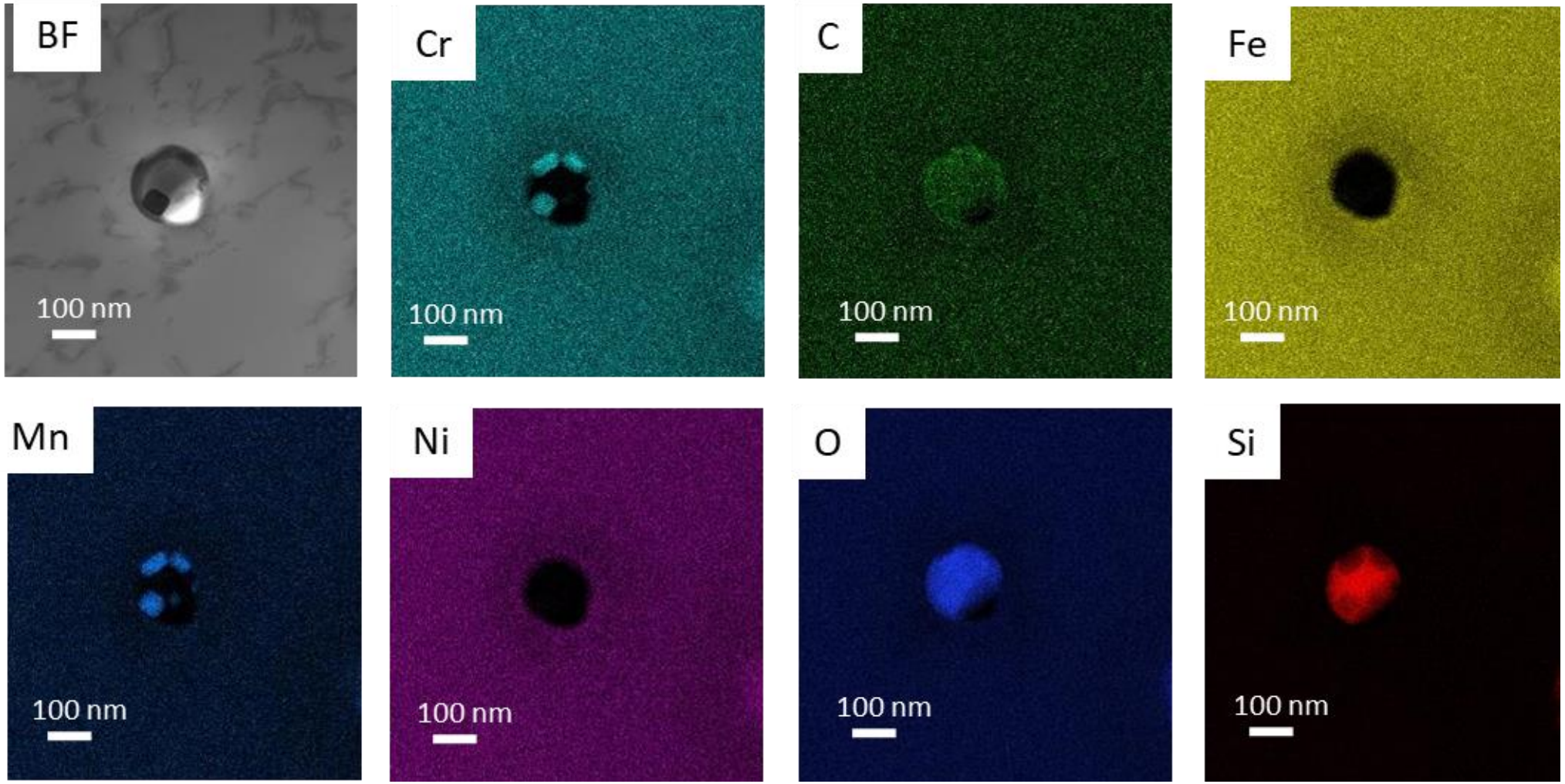

AM 316L Pristine

Finding highlight #2: Processing-introduced pores contain amorphous filling.

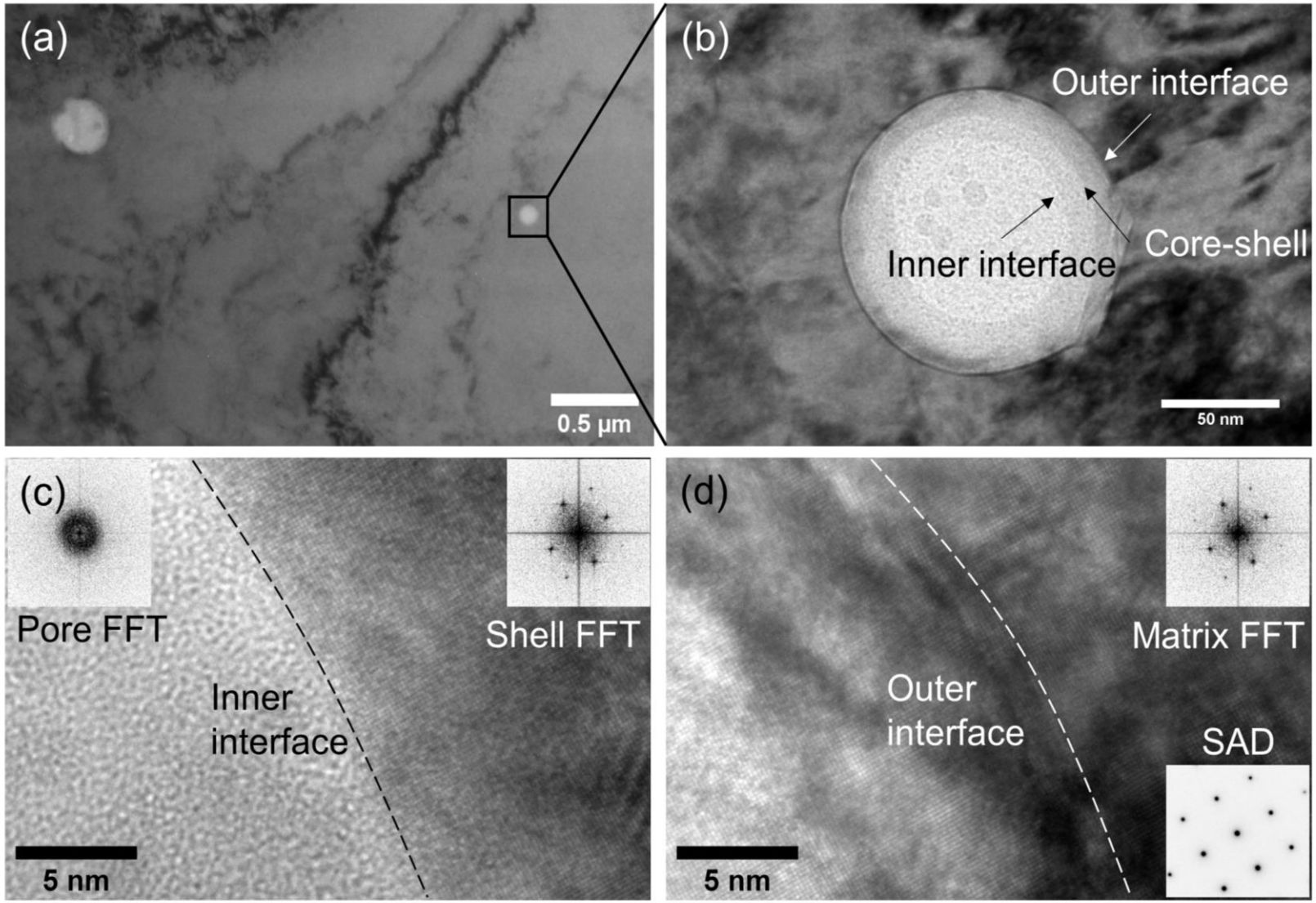

Finding highlight #3: Tensile strain around pore edges

Strain mapping of AM 316L Pristine

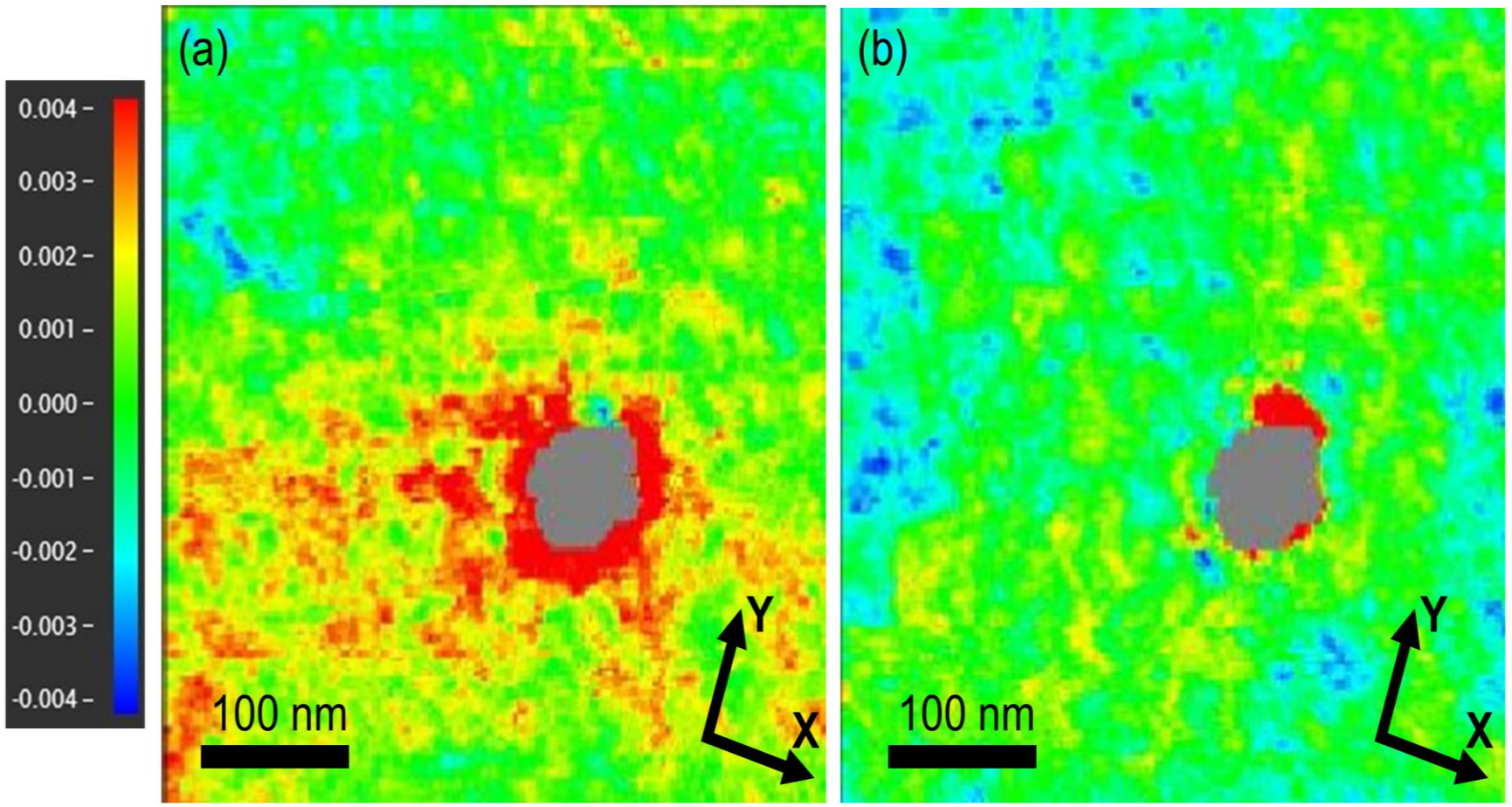

Finding highlight #4: Pore-twinning interaction and local phase changes around pores

Deformed AM 316L Pristine

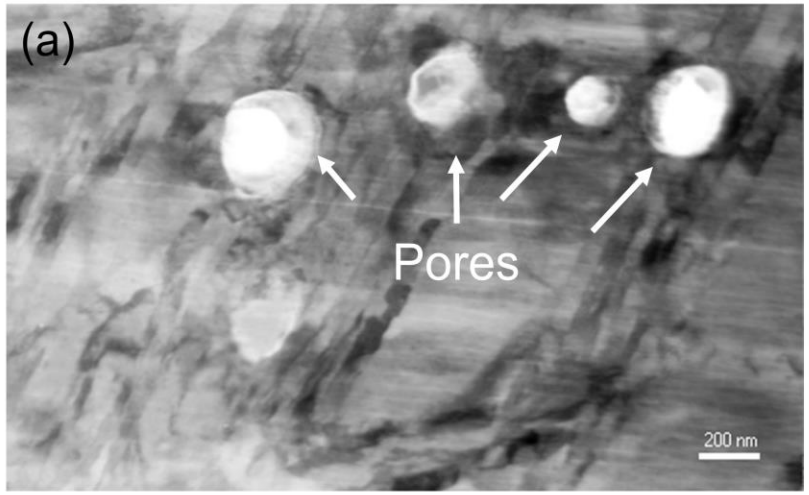

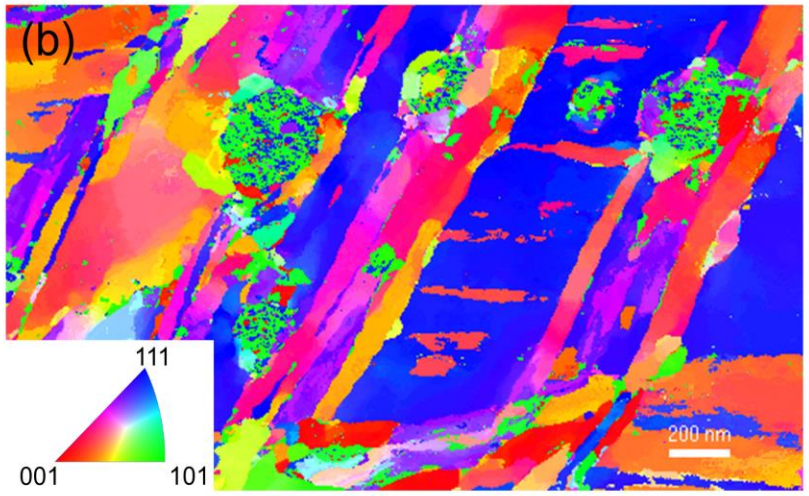

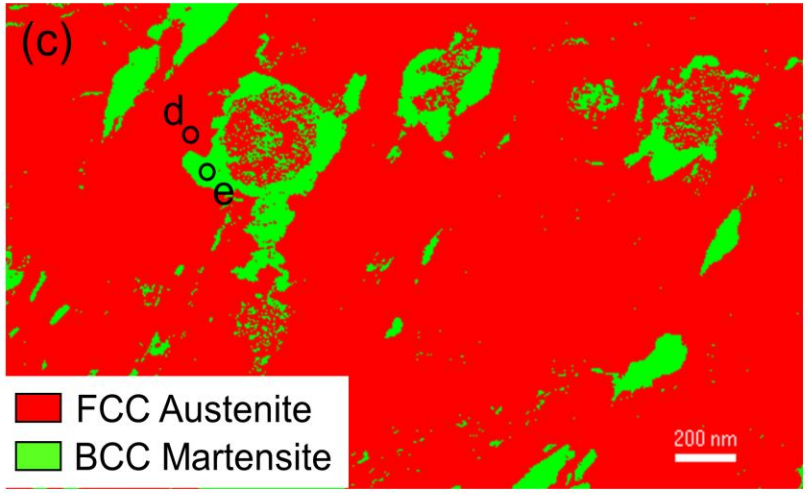

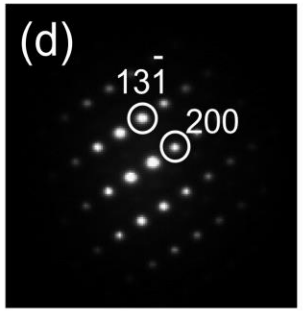

Z = [012]

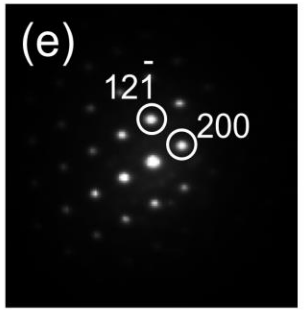

Z = [013]

Finding highlight #5: Irradiation-induced elemental segregation around dislocations

AM 316L after 5 dpa 2 MeV proton irradiation

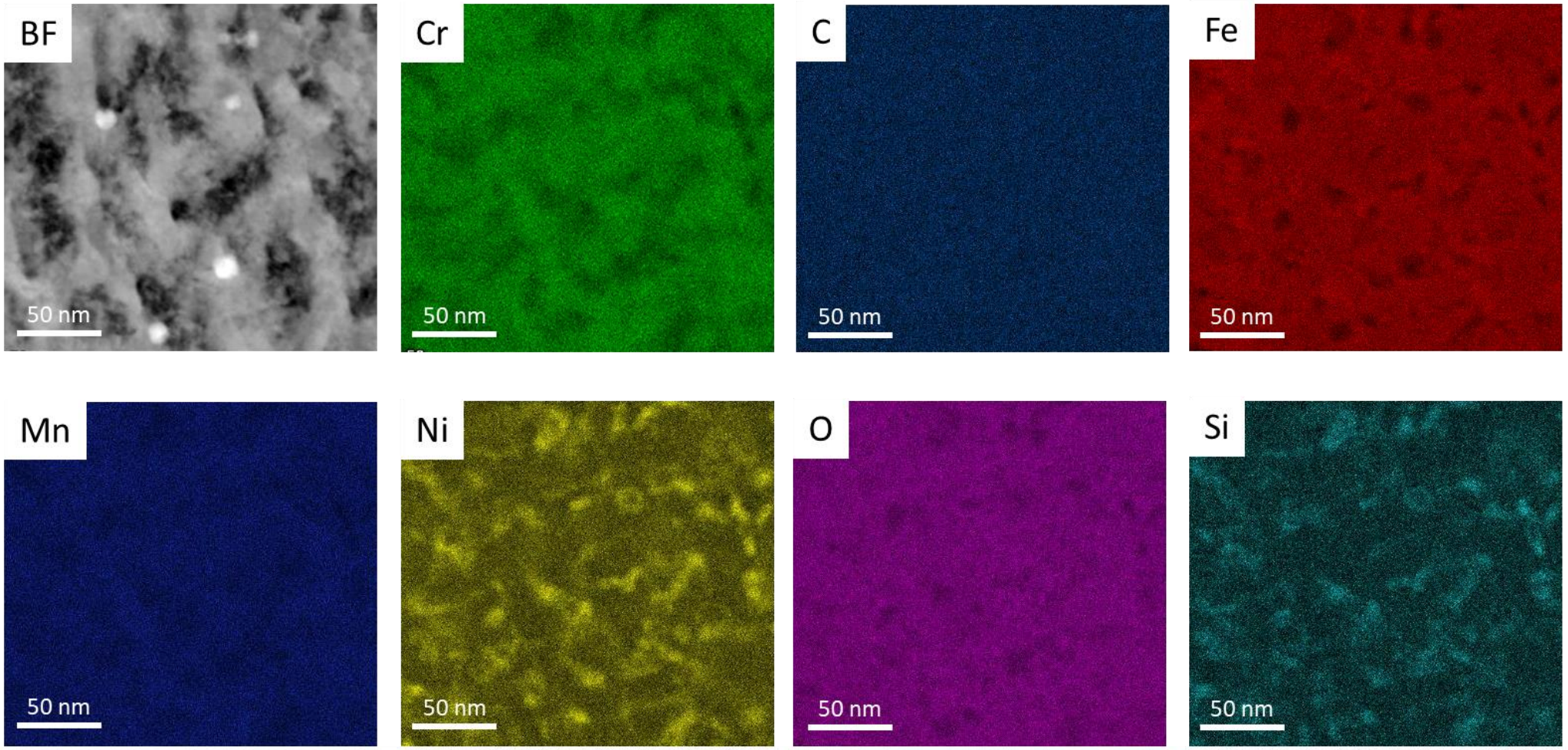

Finding highlight #6: Irradiation-induced segregation around voids

AM 316L after 5 dpa proton irradiation

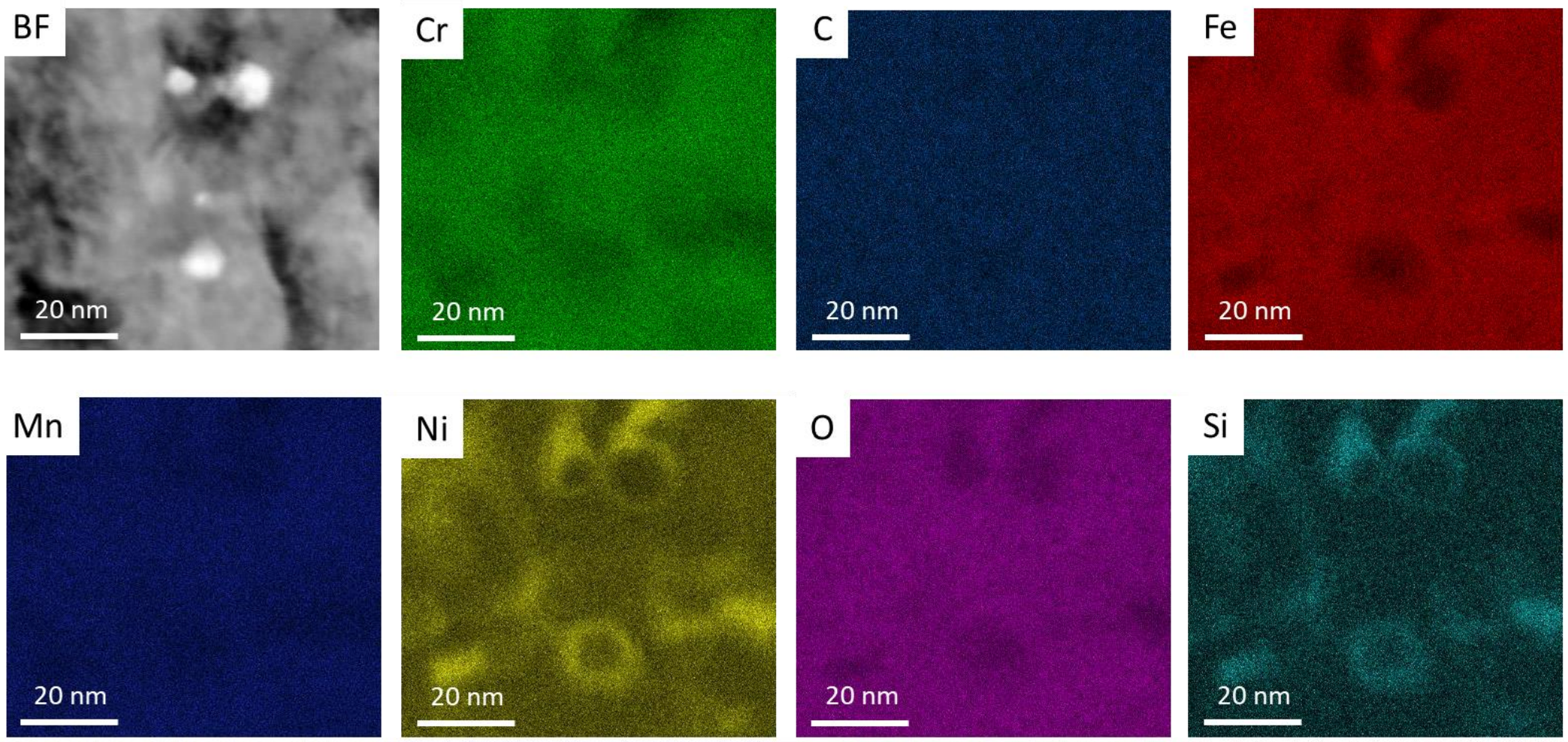

Finding highlight #7: Stabilities of grain boundaries and cell walls under irradiation

AM 316L after 220 dpa Fe self ion irradiation at 450 °C

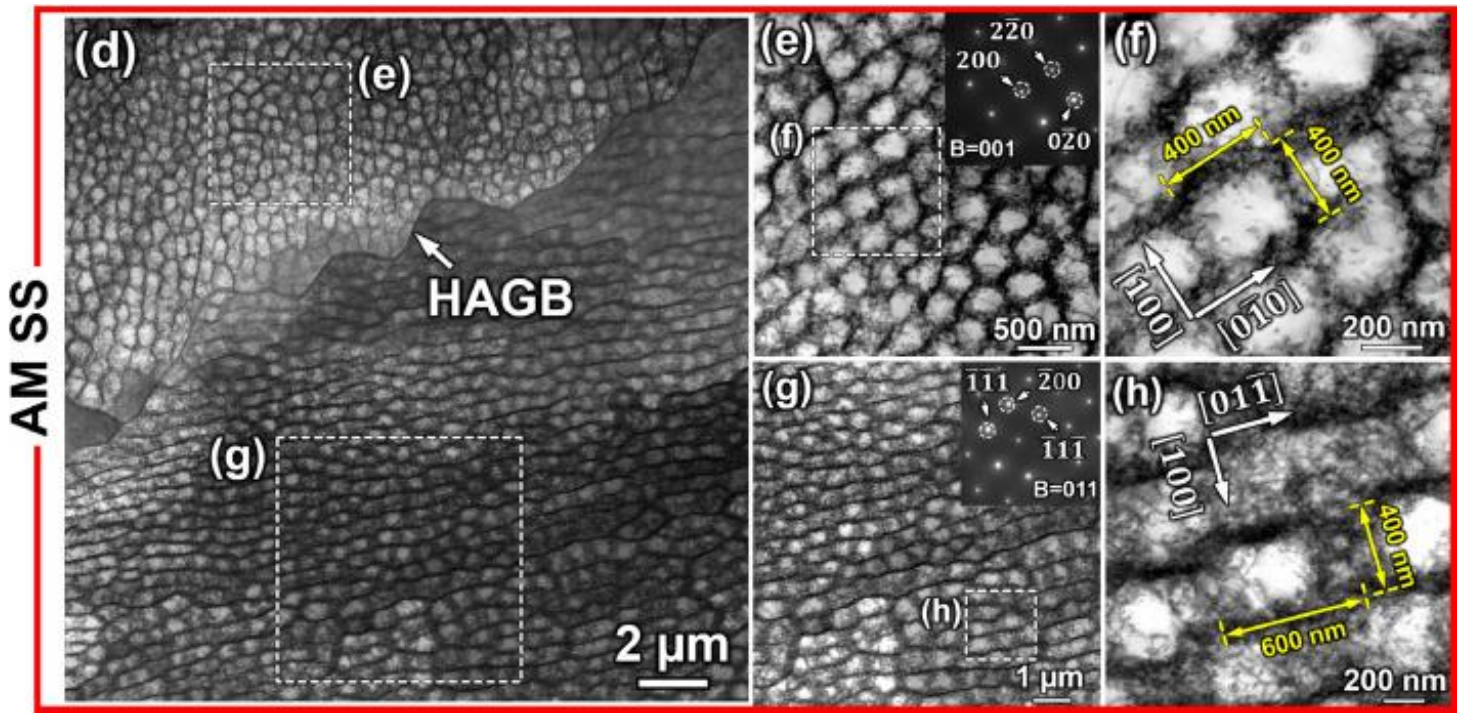

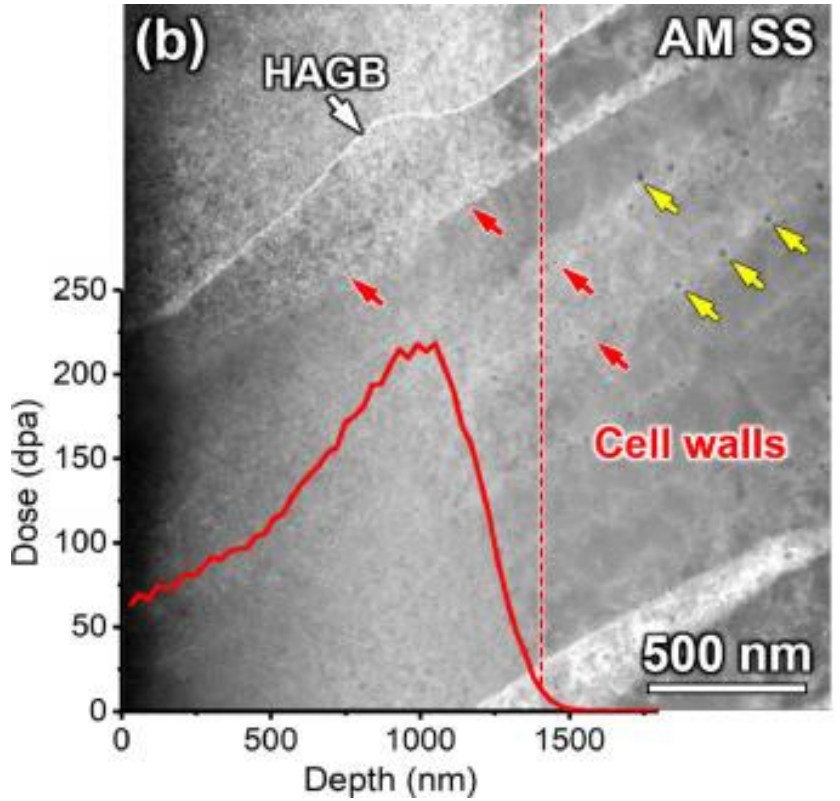

The cellular walls labeled by red arrows are still decorated with trapped dislocations and mostly Si-rich precipitates marked by yellow arrows.

Finding highlight #8: Element segregation difference between grain boundaries and cell walls after irradiation

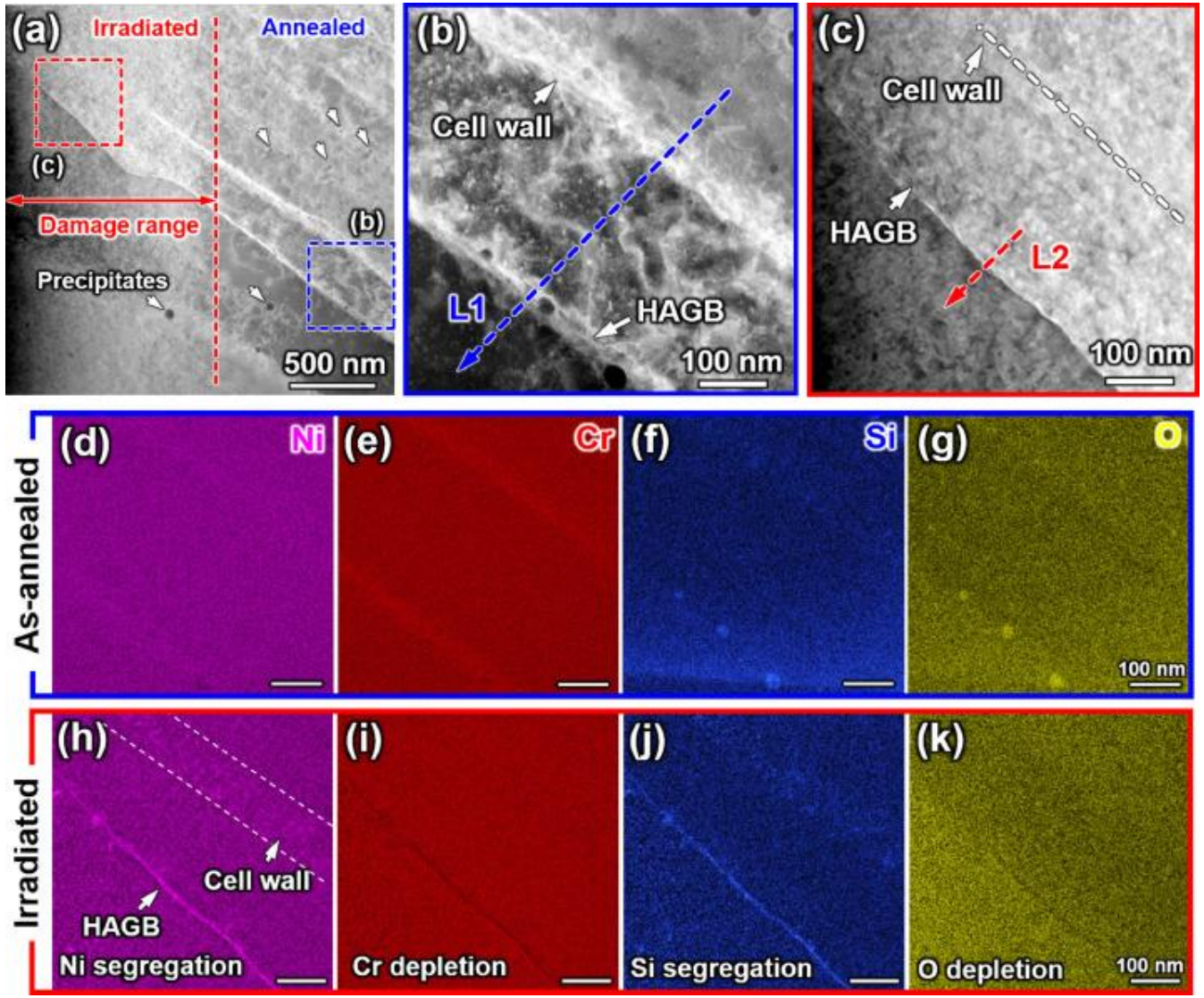

AM 316L after 220 dpa Fe self ion irradiation at 450 °C

After irradiation, the HAGB experienced prominent localized Ni and Si segregations and Cr depletion. In contrast, the cellular wall had weak Ni and Si segregation and insignificant Cr depletion.

Finding highlight #9: Cr enrichment changes to Cr depletion upon irradiation

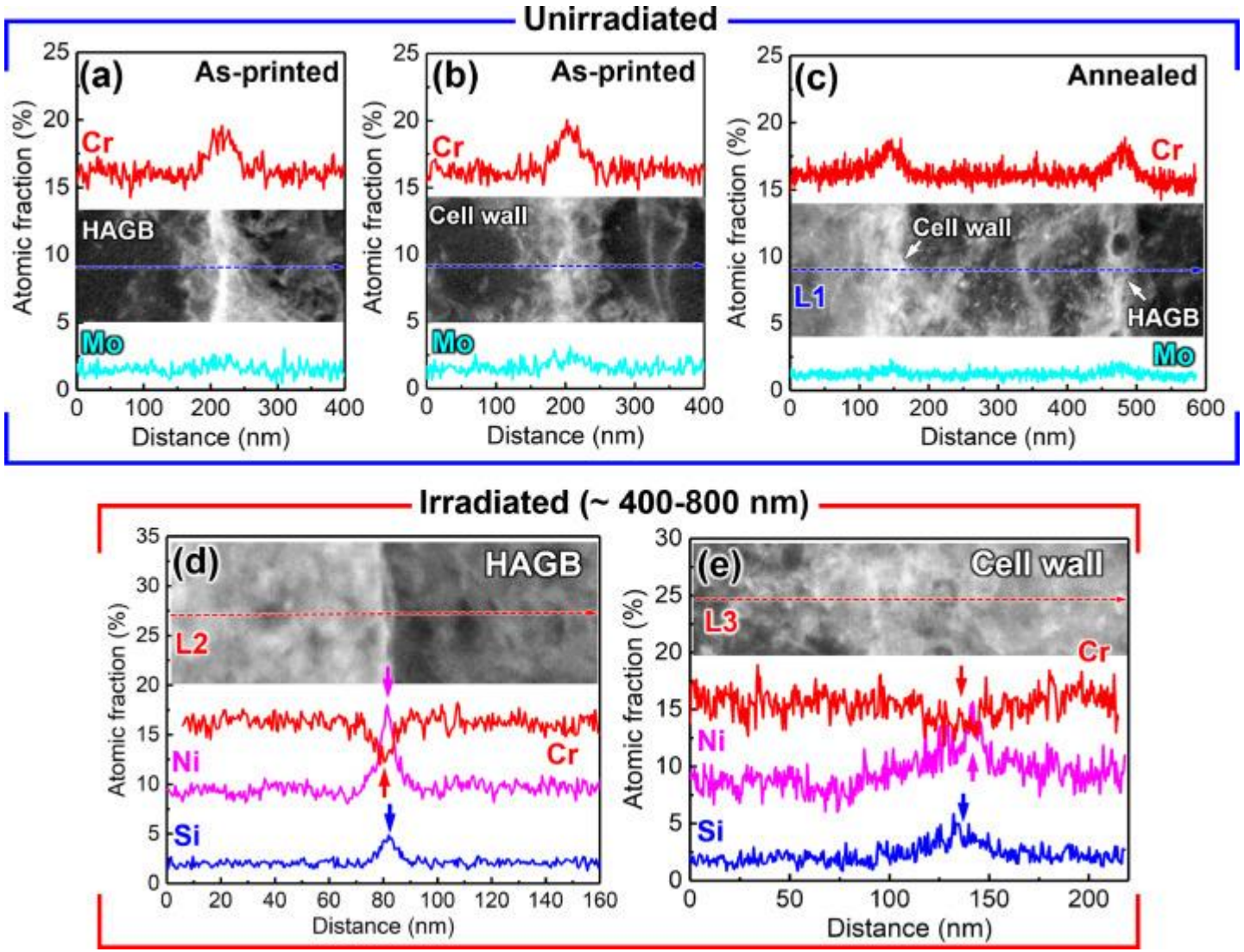

AM 316L after 220 dpa Fe self ion irradiation at 450 °C

Irradiation generated Ni and Si segregations and Cr depletion along the HAGB and cellular wall. Whereas the magnitude of Ni and Si segregation and Cr depletion along the cellular wall appears much less across a broader region.

Finding highlight #10: AM alloys swell less than the wrought counterparts

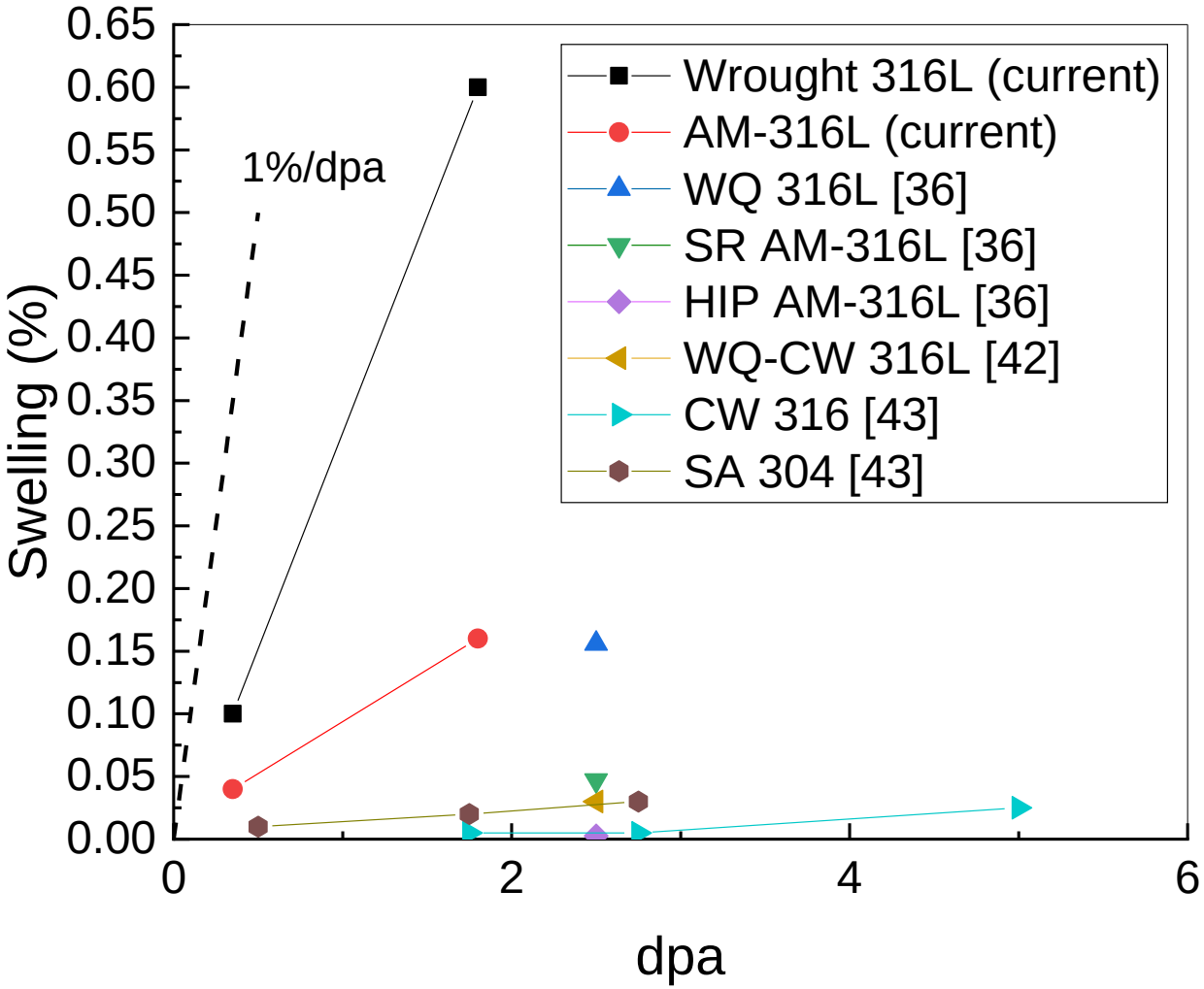

AM 316L after proton irradiations

It is a consistent observation that AM alloys swell less than the wrought counterparts. This can be due to their complicated grain/cell structures or due to impurities such as H and C.

Finding highlight #11: Residual stress can be removed by annealing.

Comparison of as-manufactured, annealed, and proton-irradiated AM 316L variants

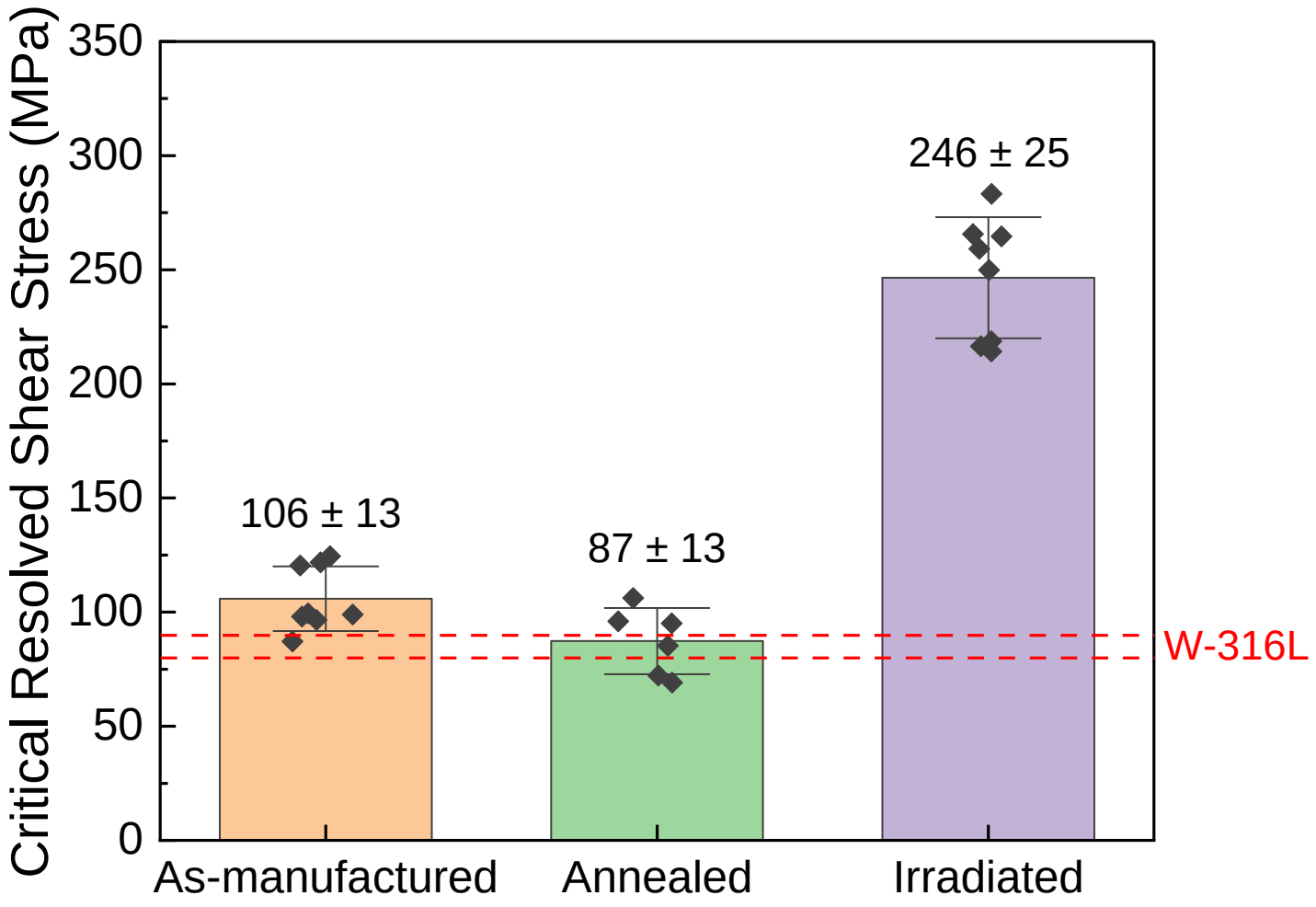

Comparison of critical resolved shear stress for as-manufactured, annealed, and irradiated AM-316L variants. The bar heights represent the average values for each variant. The red dashed lines refer to the range of literature-reported values of wrought 316L SS.

Residual stress/strain induced by processing causes hardening. The stress can be removed by annealing.

Radiation hardening is mainly contributed by irradiation-induced dislocation loops.

Recent progress on in situ micro-pillar compression on the cross sections of proton irradiated additively manufactured 316L stainless steels

Motivation

- **Purpose: Understanding irradiation responses and mechanical properties of AM alloys due to unique microstructures introduced**
- **For the present study: A micropillar compression study with two different approaches (planar pillars vs. cross-sectional pillars) was performed on proton irradiated additively manufactured AM 316L stainless steels.**

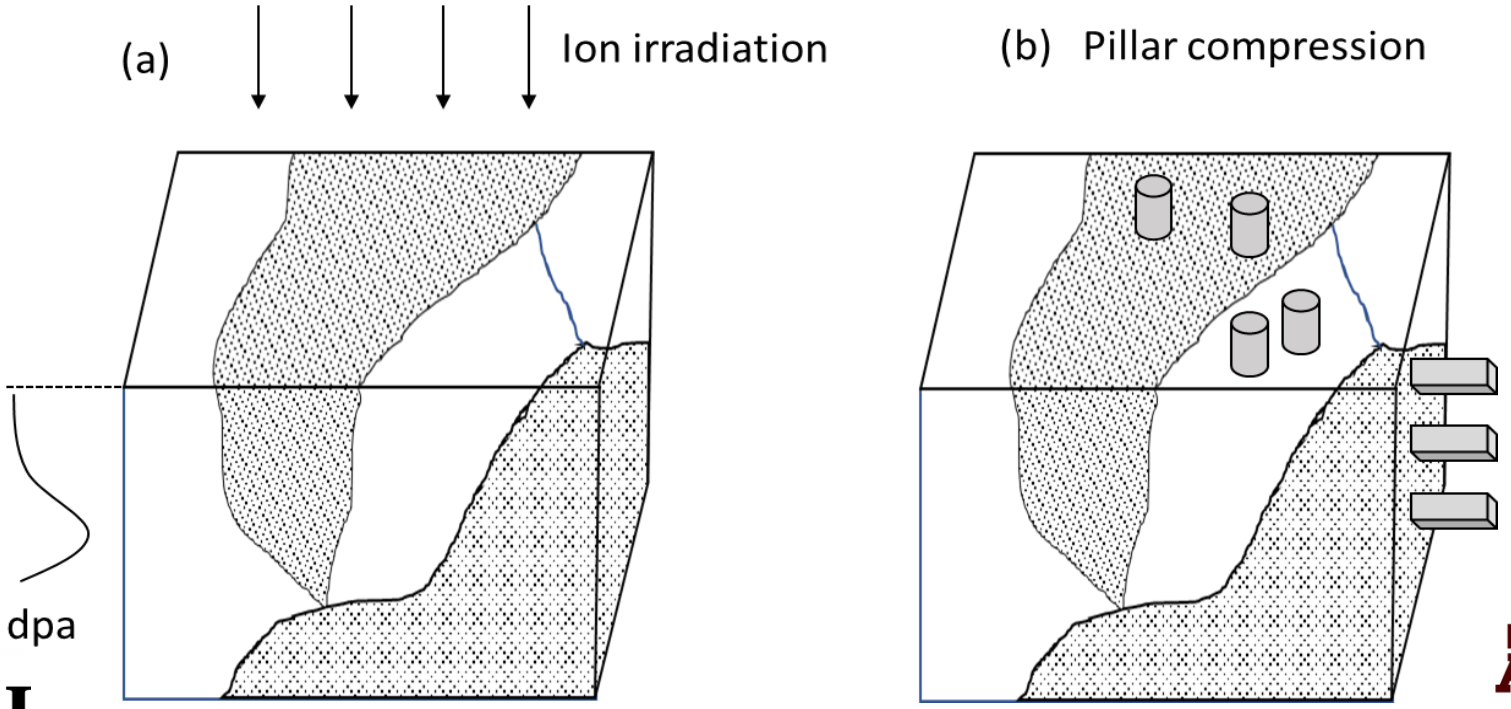

Irradiation damage by 2 MeV protons

(a) Voids

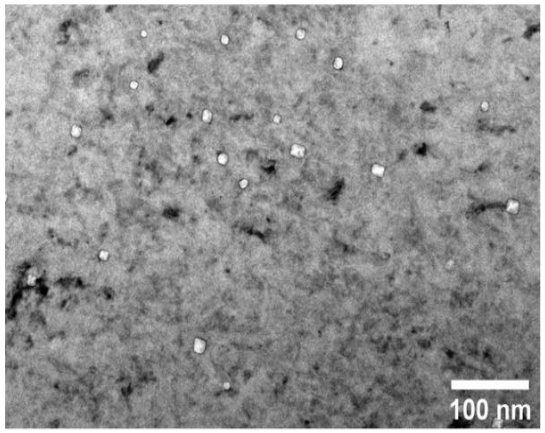

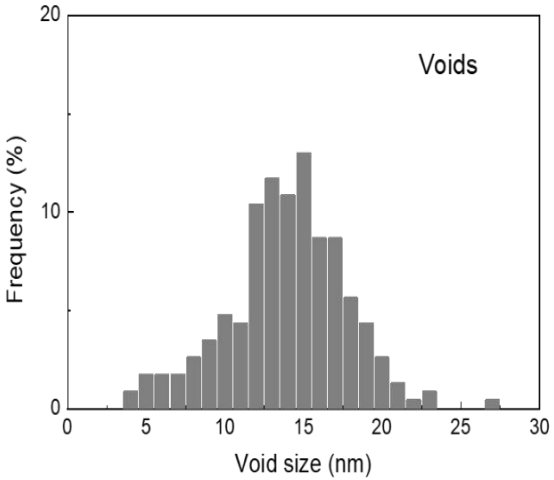

(b) Dislocation loops

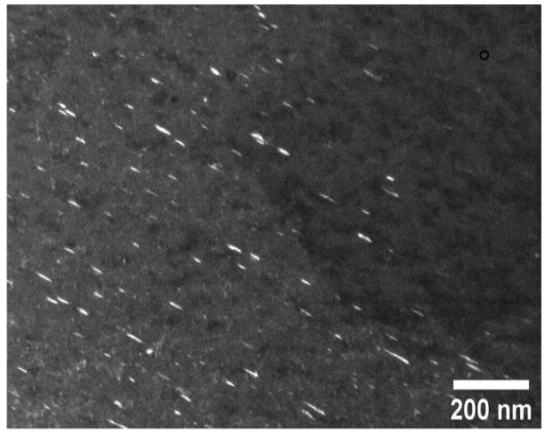

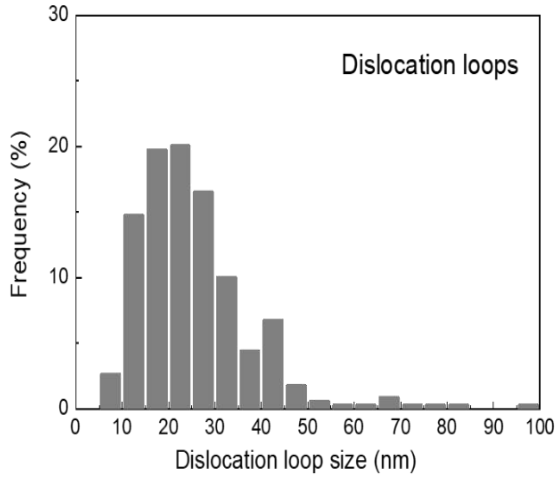

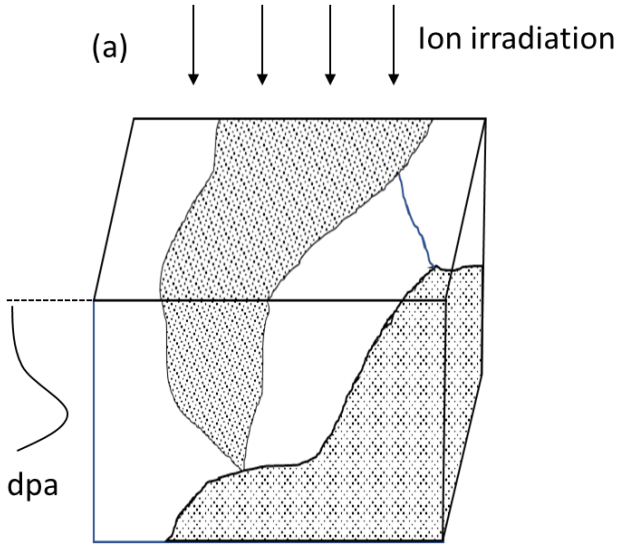

Planar pillar compression

- **Planar pillars**: **Orientation-selected, 5 μm in diameter and 10 μm in height**

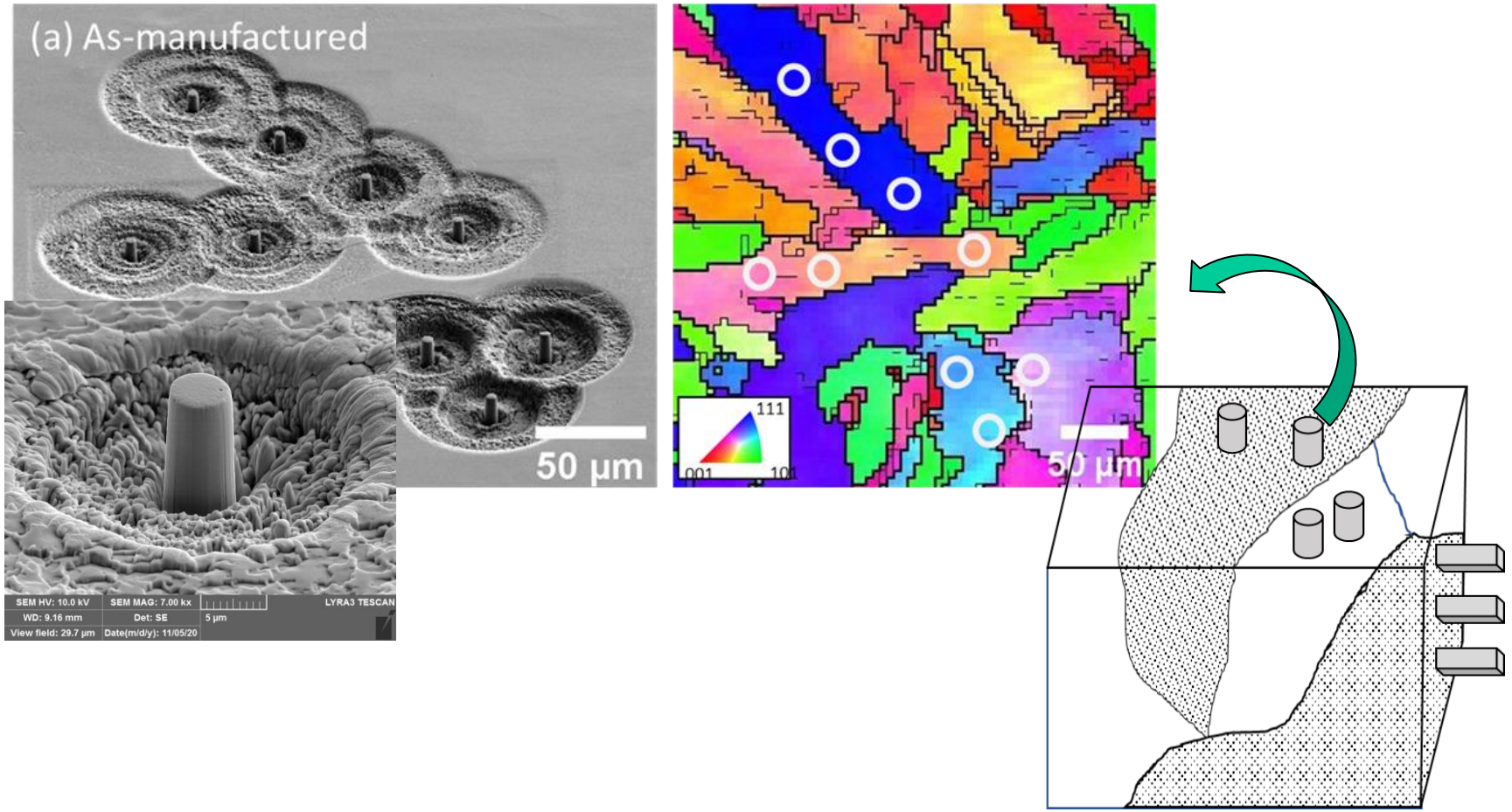

Orientation-selected Micro-pillar Compression

- **Stress was converted to resolved shear stress on the slip plane.**

$$\tau = \sigma \cos\lambda\cos\phi = \sigma m$$

m : Schmid factor

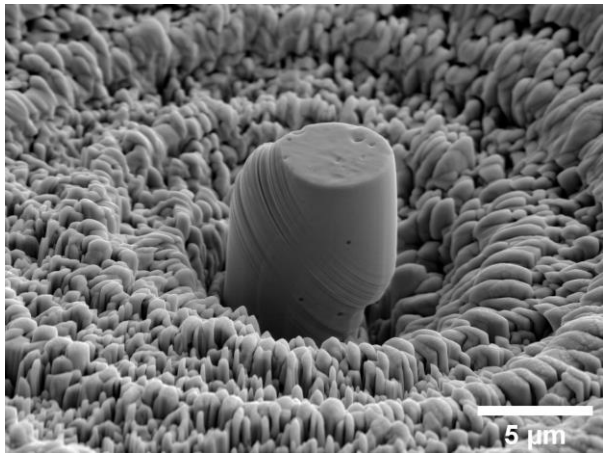

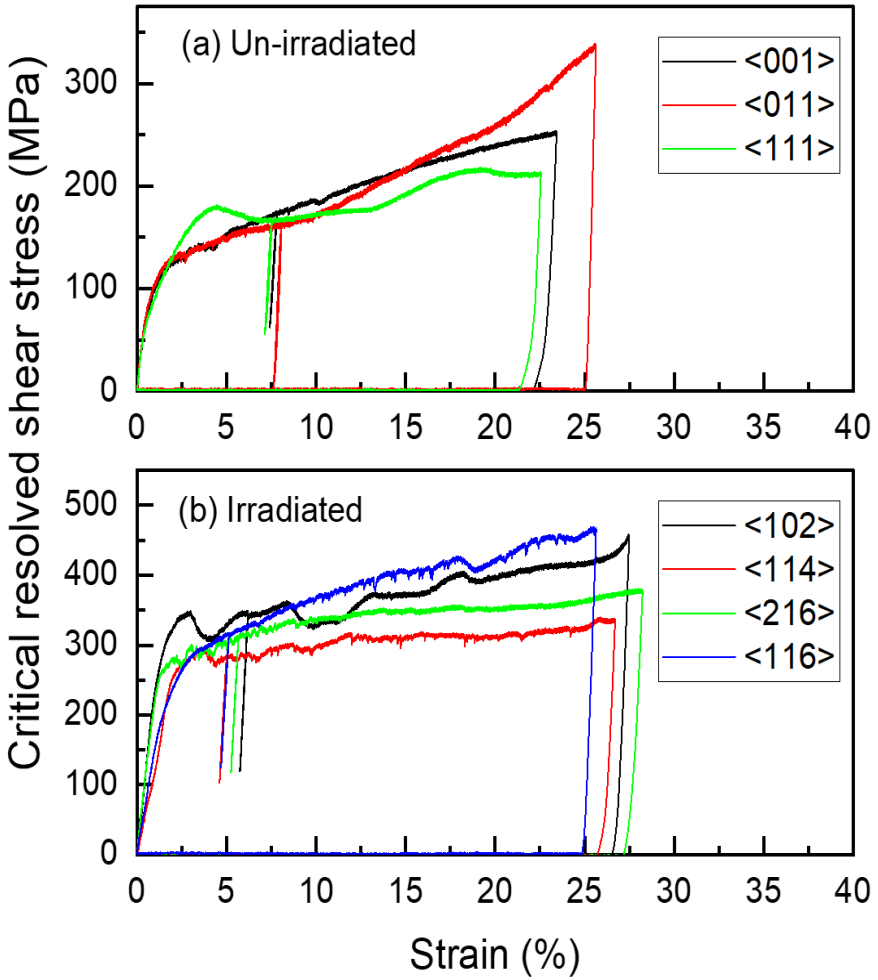

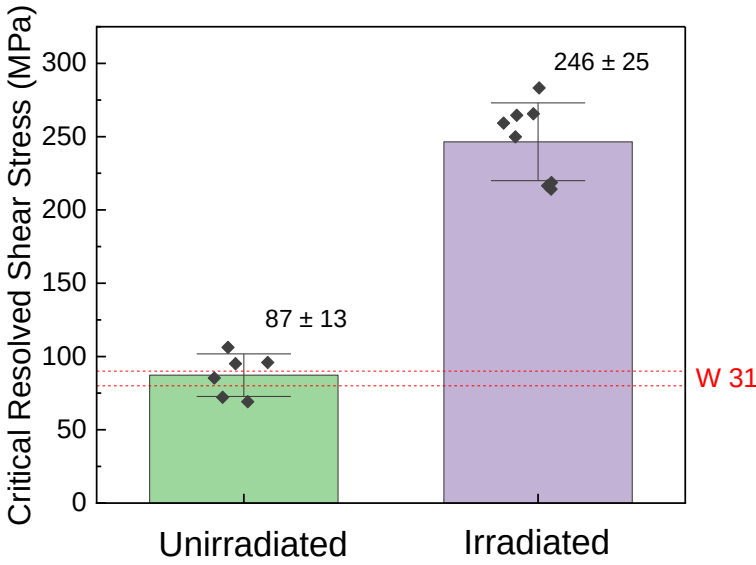

Significant irradiation hardening was observed.

Finding highlight #12: Deformation mechanism switches from dislocation gliding (in as-manufactured) to twinning (proton-irradiated)

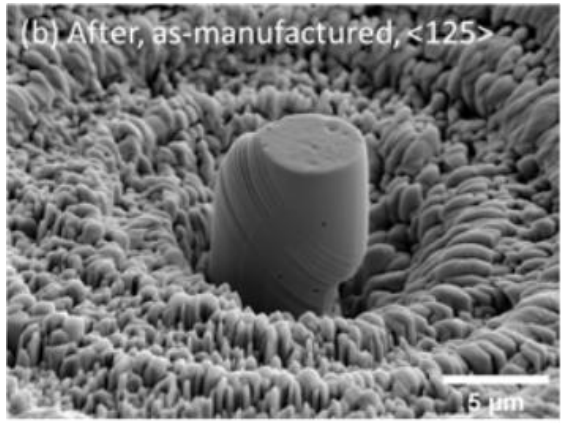

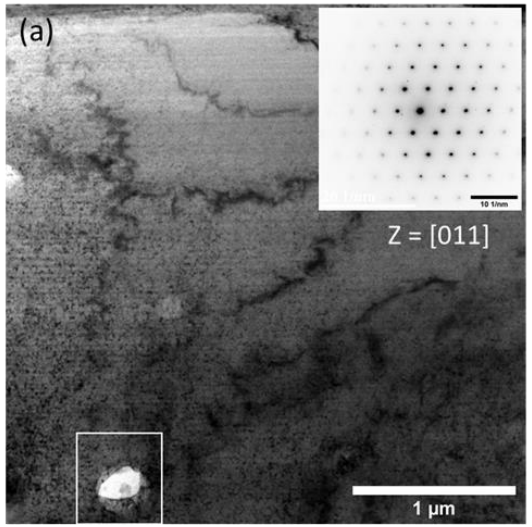

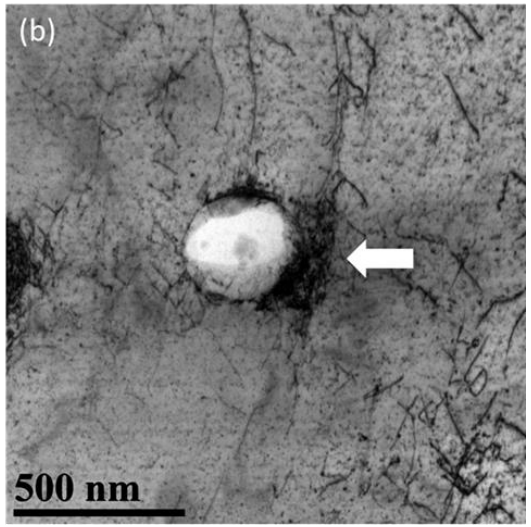

As-manufactured AM 316L

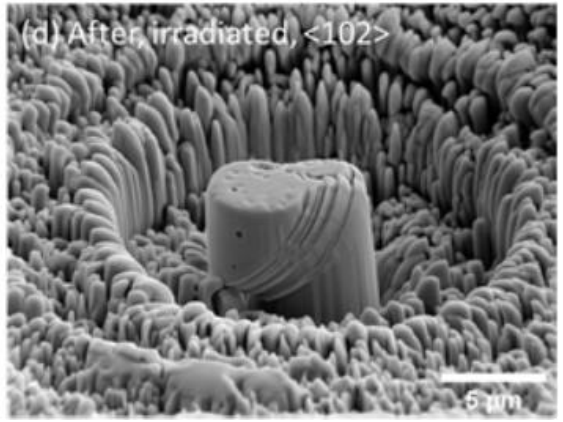

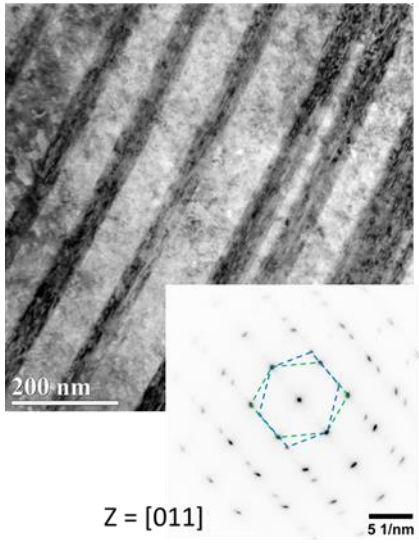

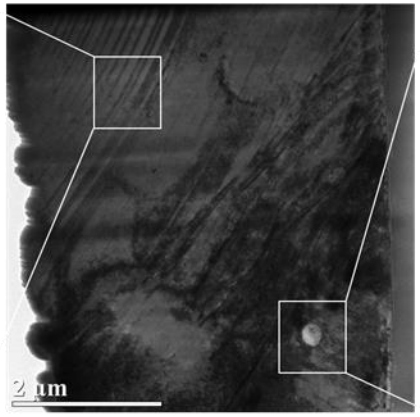

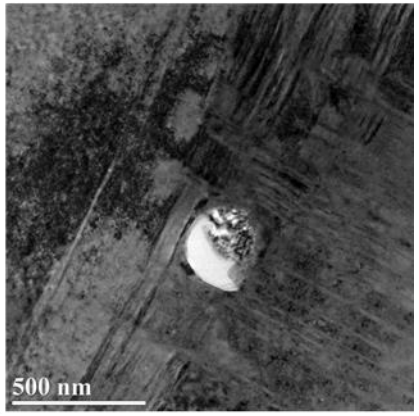

Proton-irradiated AM 316L

Reducing dpa uncertainty using cross-sectional pillar compression

- **Motivation:** **Can cross-sectional pillars obtain better local dpa dependence, with reduced dpa uncertainty?**

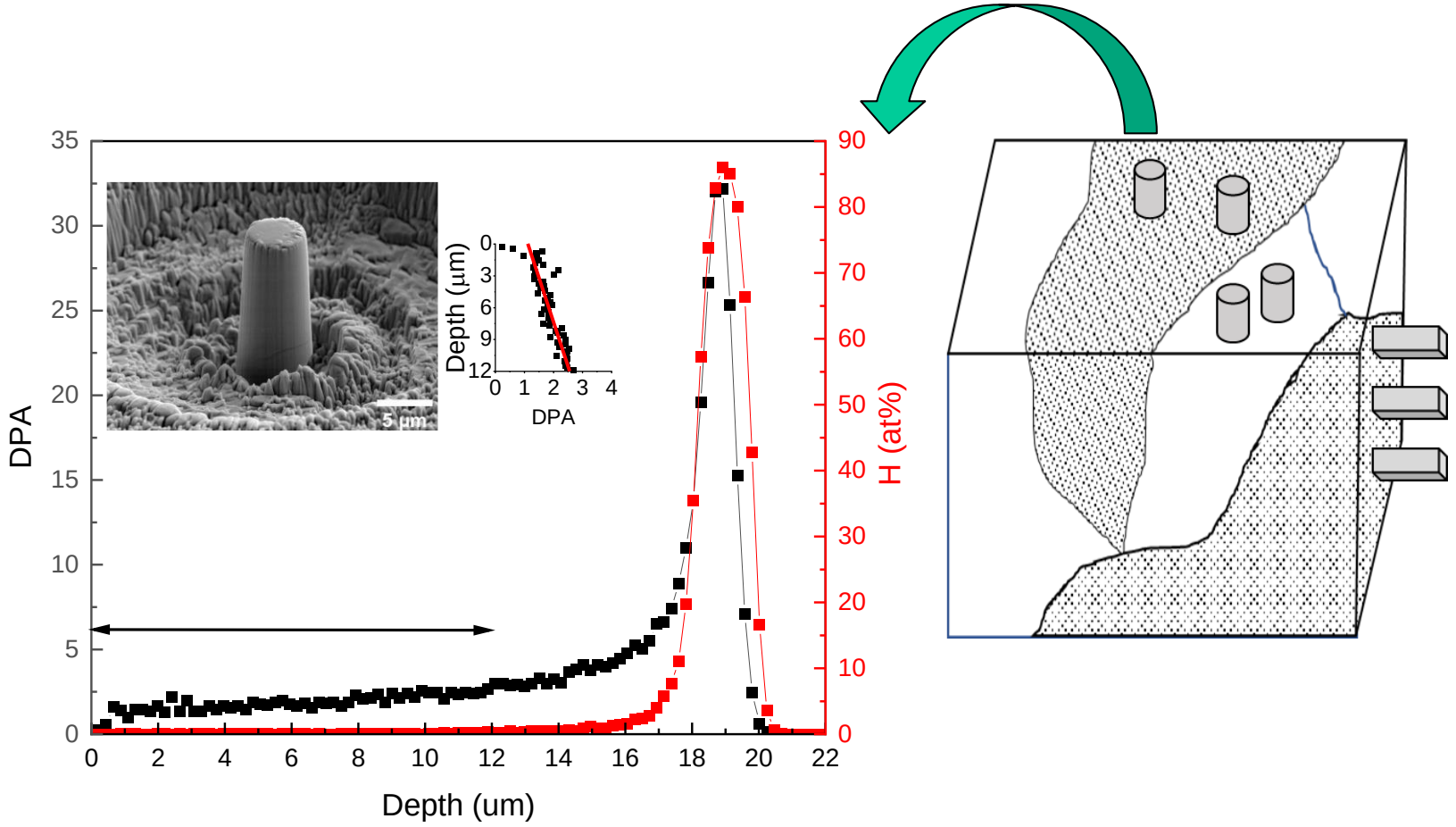

Cross-sectional pillars

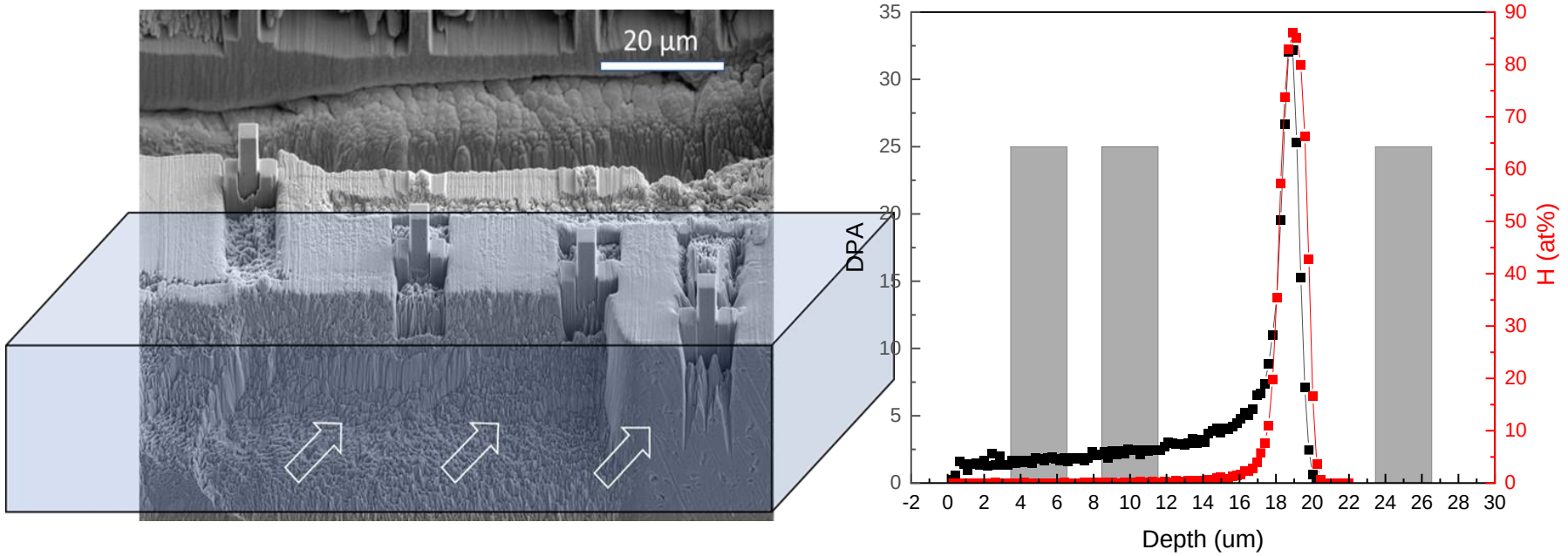

Pillars were prepared on the cross section of the irradiated sample. All pillars were located within one grain. The arrows refer to the proton beam direction.

In situ pillar compression of cross-sectional pillars

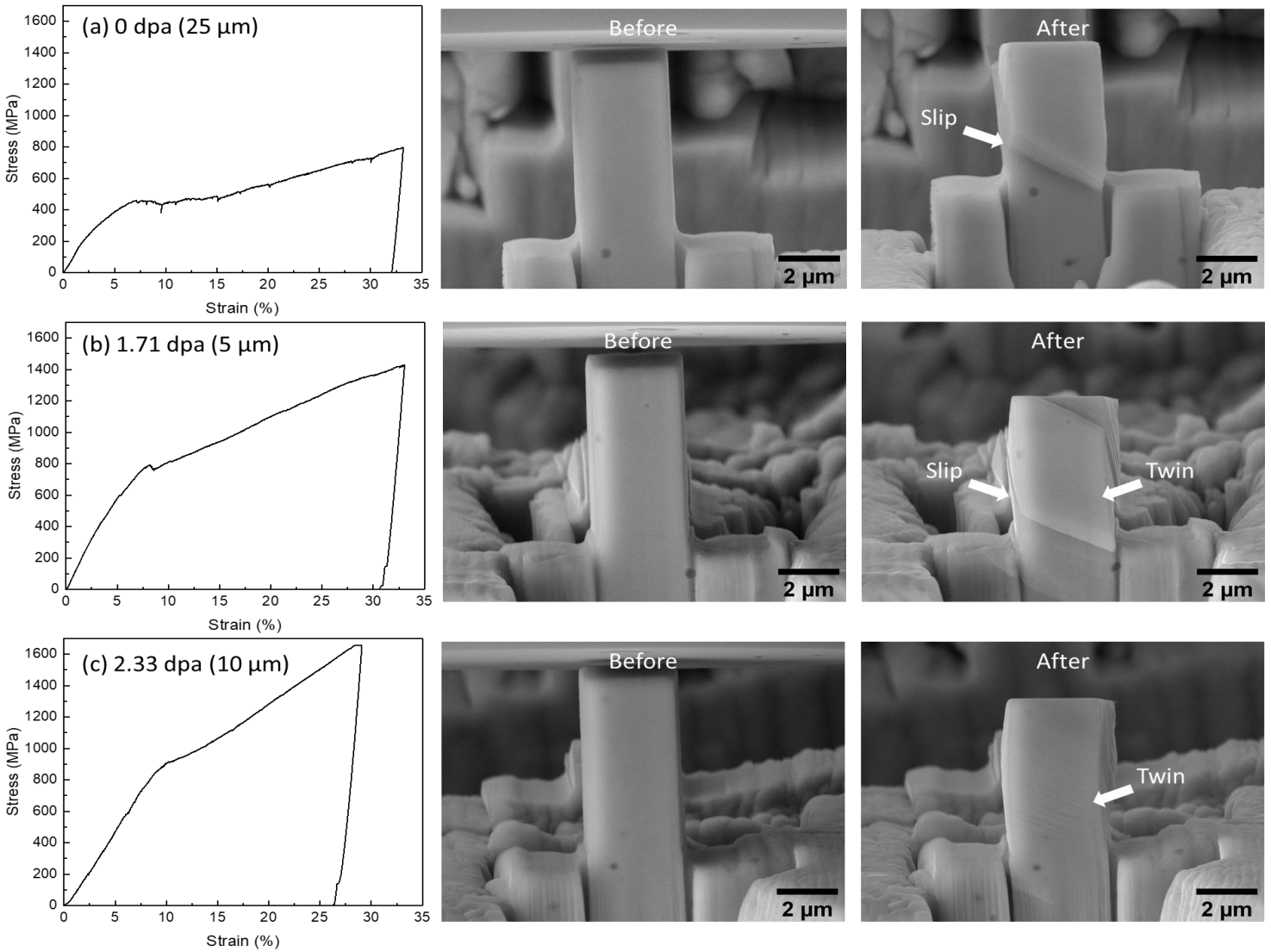

Post-compression pillar characterization
0 dpa (the deepest pillar)

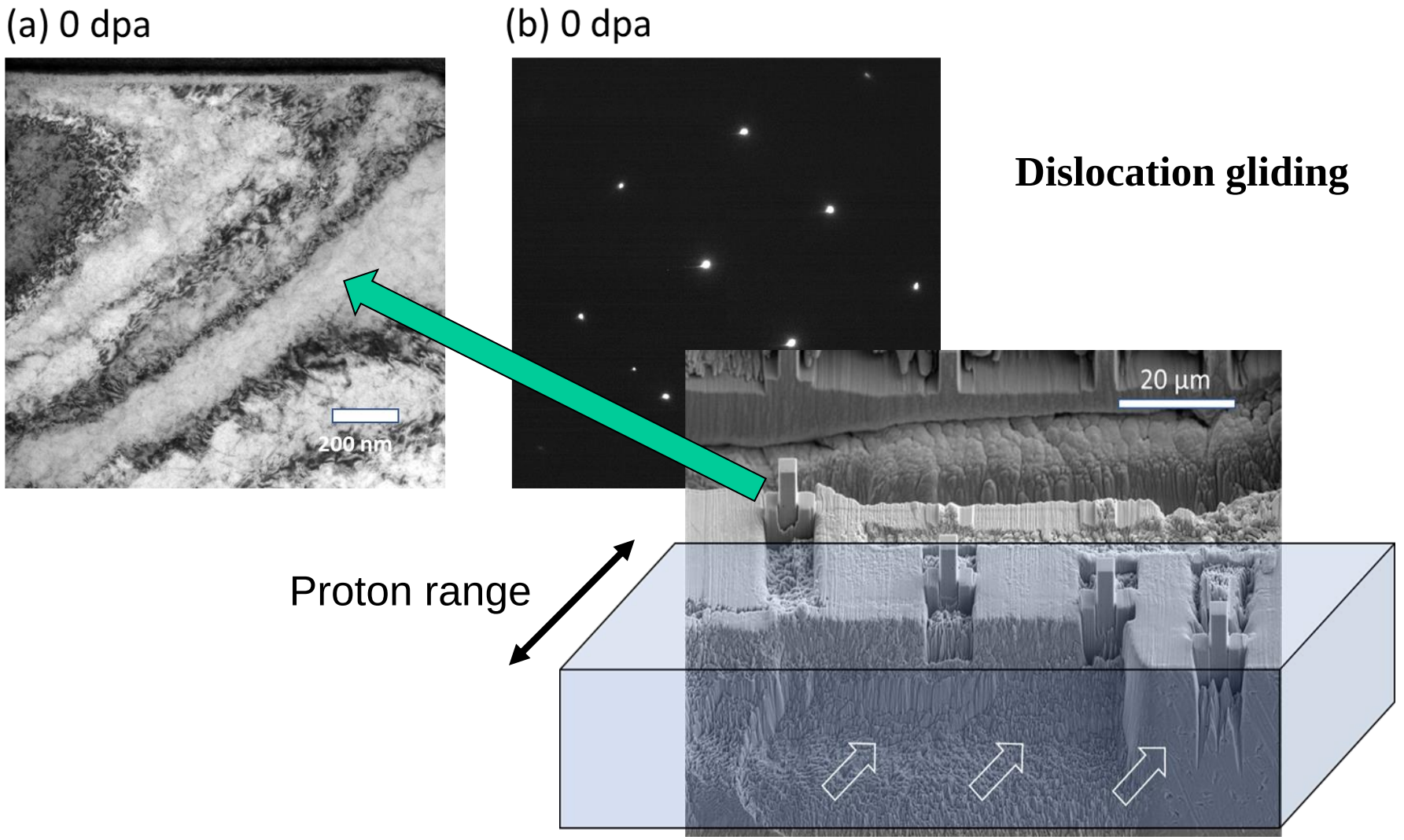

Post-compression pillar characterization
1.71 dpa pillar (the shallowest)

(a) 1.71 dpa

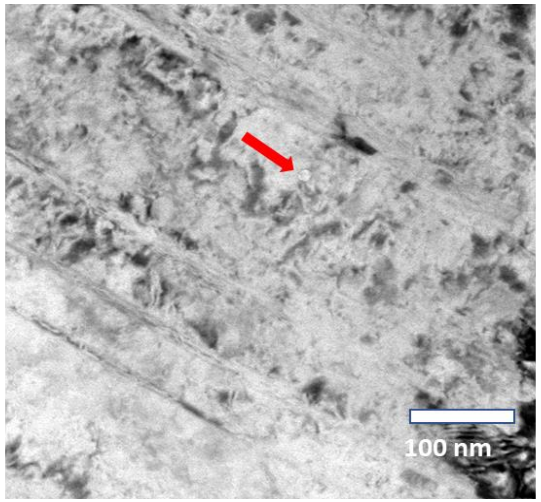

(b) 1.71 dpa

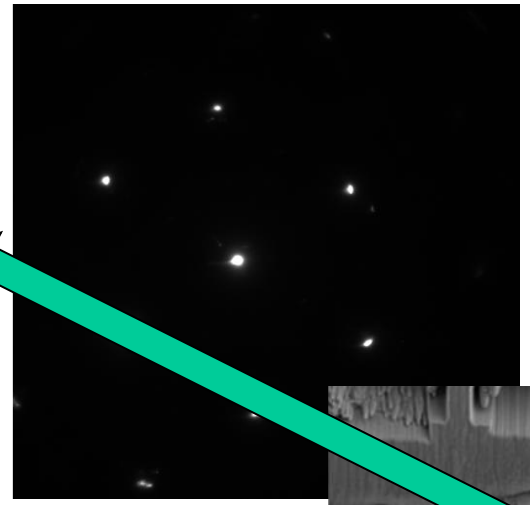

A mixture of dislocation gliding and twinning

TEM image and diffraction pattern obtained from the compressed 1.71 dpa pillar.

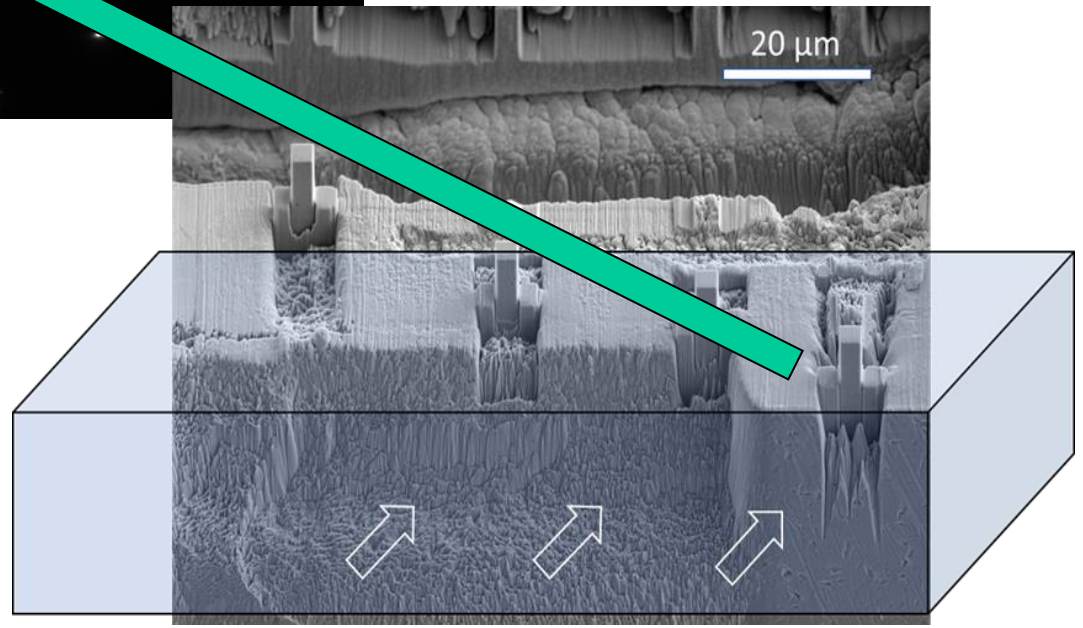

Post-compression pillar characterization
2.33 dpa pillar (at deeper depth)

(a) 2.33 dpa

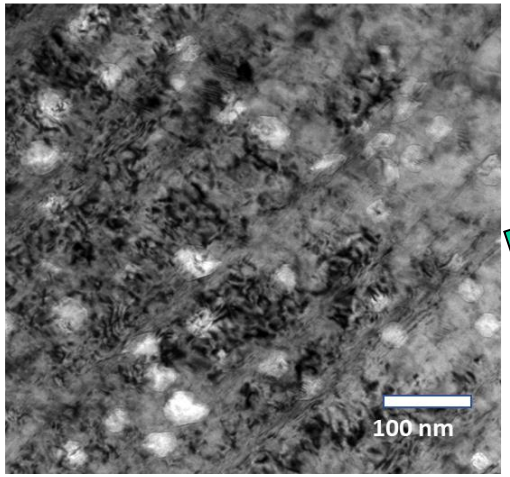

(b) 2.33 dpa

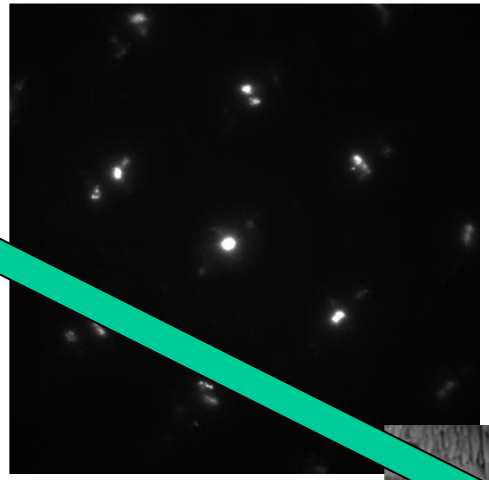

Twinning

TEM image and diffraction pattern obtained from the compressed 2.33 dpa pillar.

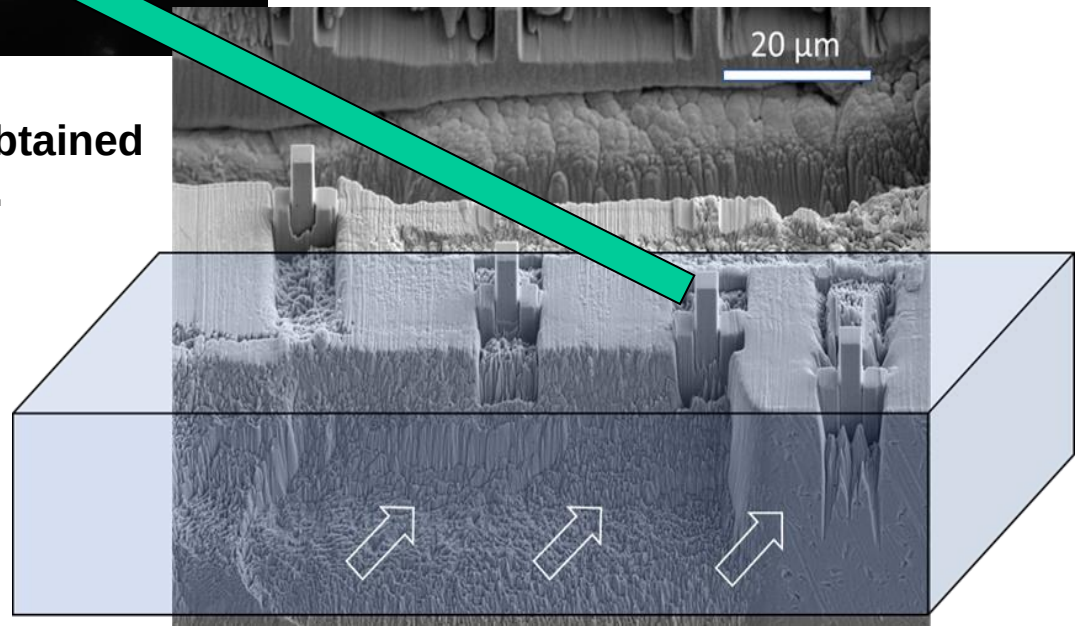

Why twinning?

- **Dissociation of dislocation into Shockley partial dislocations creates twin boundaries.**
- **In austenitic alloys, dissociation happens on the (111) plane from the Burgers vector of $a/2 < 1 - 10 >$ into $a/6 < 2 - 1 - 1 >$ and $a/6 < 1 - 21 >$.**

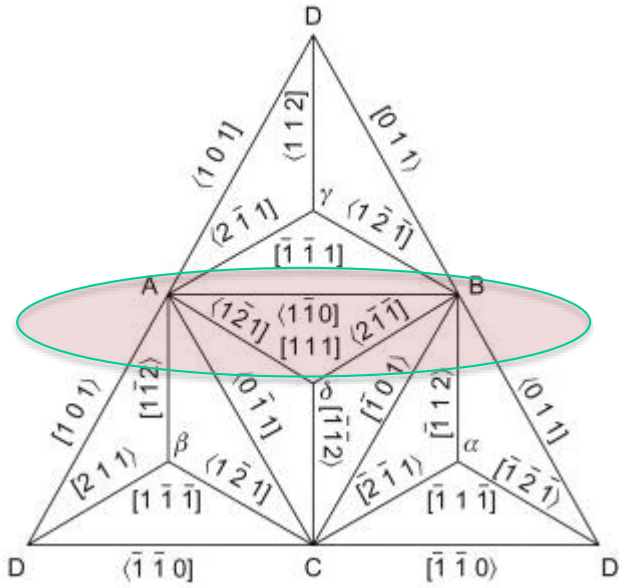

- Dissociation will occur when the external shear stress is greater than the critical shear stress τ_x^{crit} to separate the partial dislocations.

$$\tau_x^{crit} = \frac{2\gamma_{SF}}{b_p}$$

- Radiation-induced defects, such as voids and dislocation loops, strengthen materials and reach the critical shear stress to form twins.

Deformation mechanisms of irradiated AM 316L SS

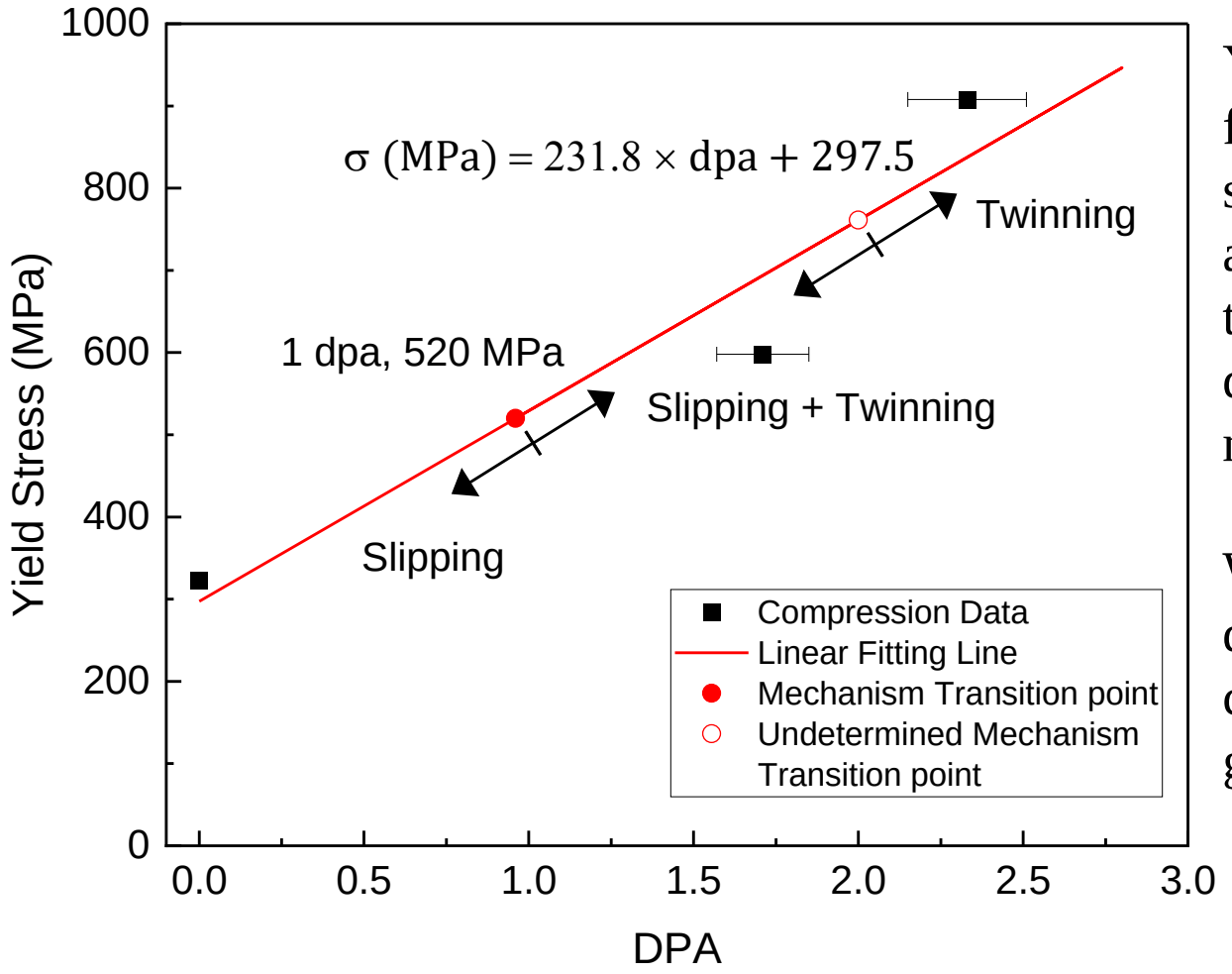

Yield stress plotted as a function of dpa value, showing the linear fitting line and the yielding mechanism transition points with the dominant deformation mechanism at yielding.

With increasing damage level, deformation mechanisms changes from dislocation gliding to twinning.

Planar vs. cross-sectional pillars

Finding highlight #13: Cross-sectional pillar compression can obtain mechanical property data with less uncertainty on dpa dependence

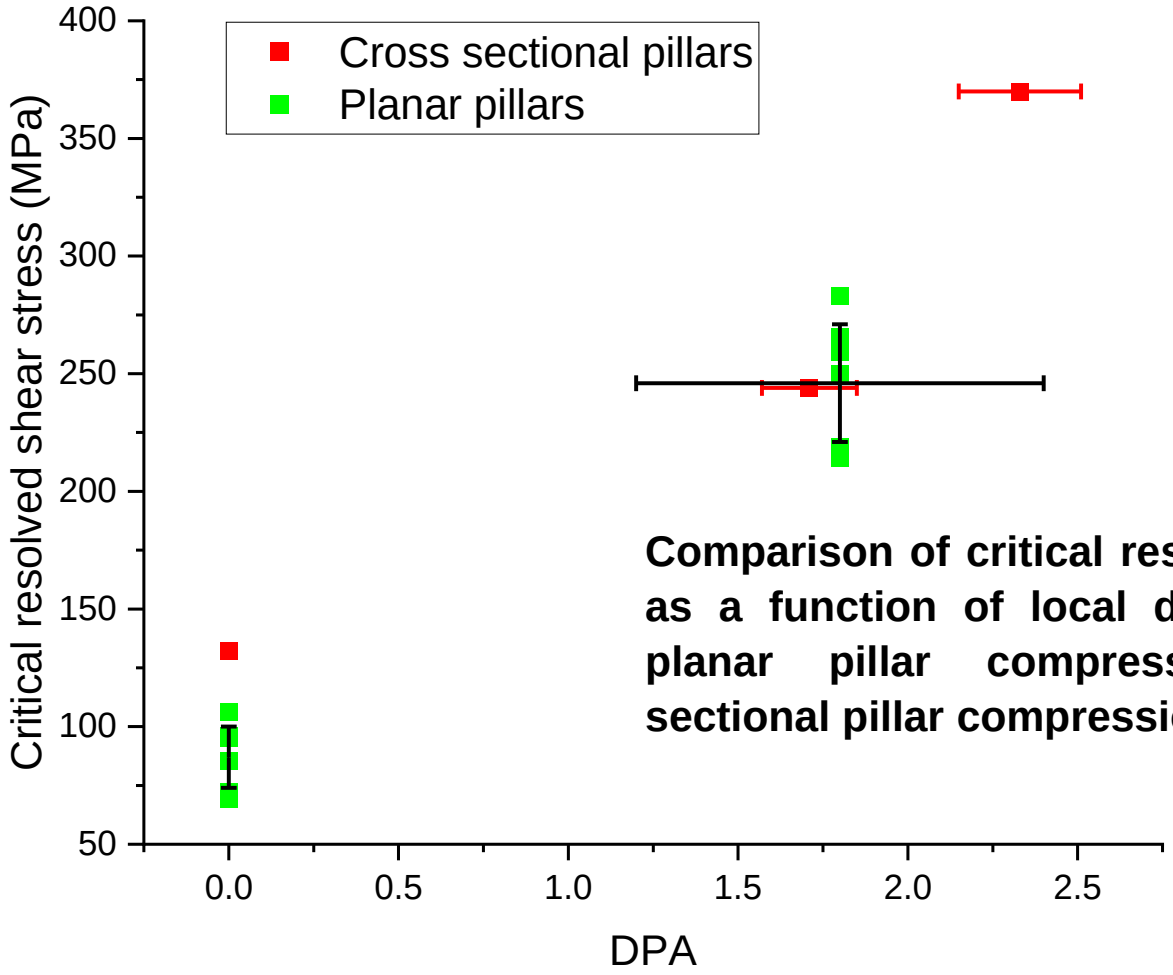

Comparison of critical resolved shear stress as a function of local dpa, obtained from planar pillar compression and cross-sectional pillar compression.

Finding highlight #14: Cross-sectional characterization over the whole irradiated region (>20 microns) is feasible to get local dpa dependent microstructural changes

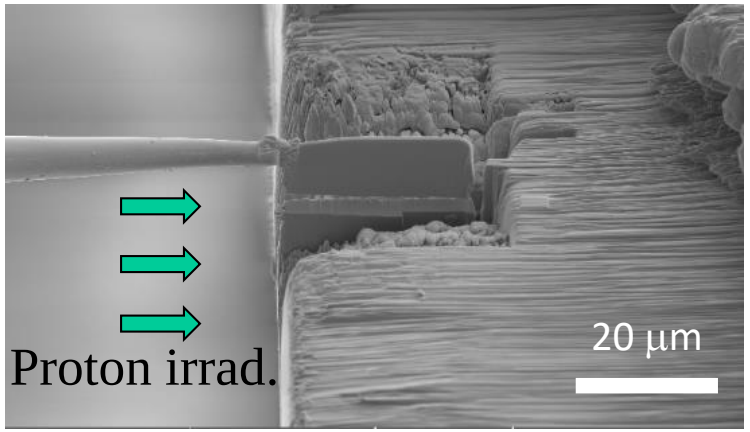

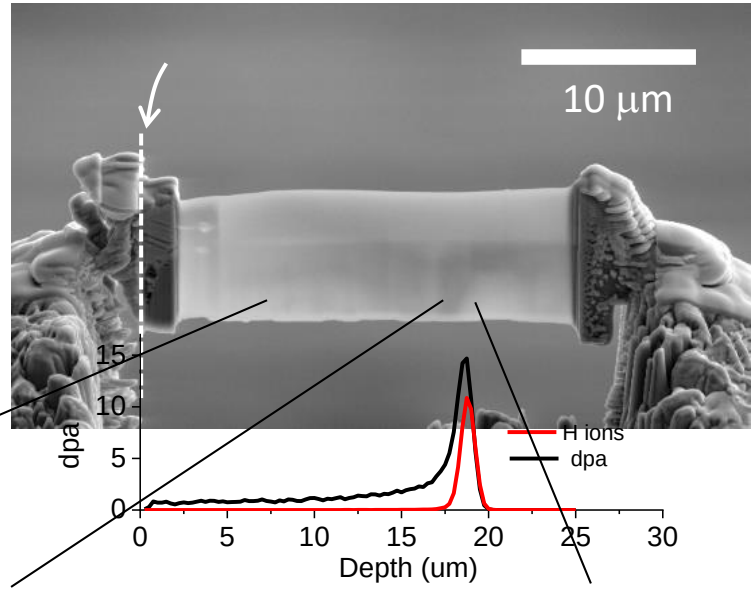

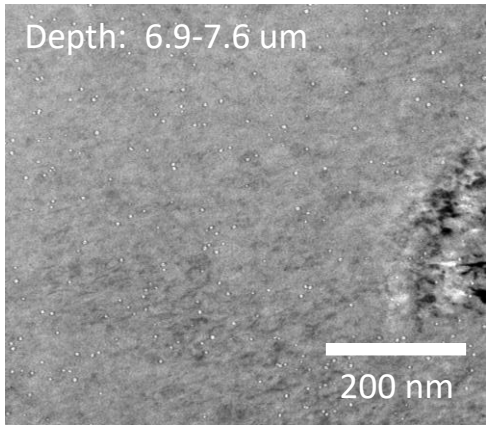

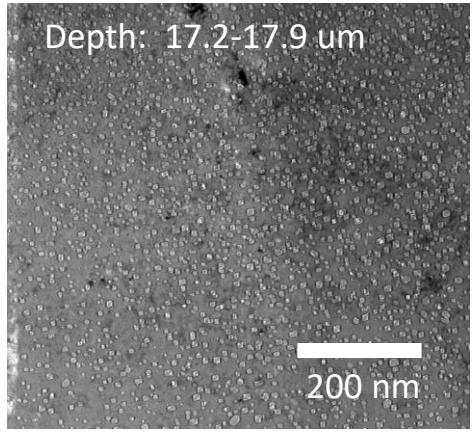

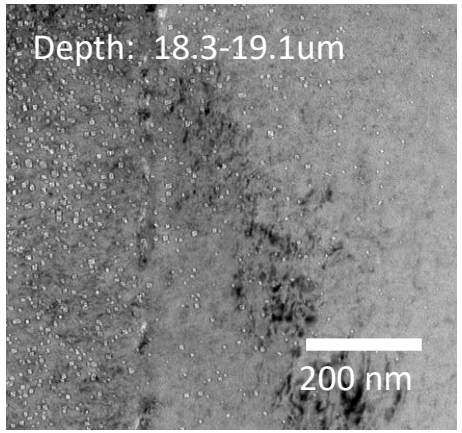

Conclusion

Addictive manufacturing introduced unique microstructures lead to unique irradiation responses and mechanical property changes.

- Atomic scale segregation
- Localized phase changes around pores
- Boundary segregation (HAGB and cell walls)
- Swelling (AM alloys swell less)
- Deformation mechanism changes (dislocation gliding $\rightarrow$ twinning after irradiation)

ACKNOWLEDGEMENTS

This material is based upon work supported by the Department of Energy / National Nuclear Security Administration under Award Number(s) DE-NA0003921.

Washington State University
Pacific Northwest National Lab
Idaho National Lab
Nevada National Security Site
Lawrence Livermore National Lab
Sandia National Labs
Lawrence Berkeley National Lab
Colorado School of Mines
The University of Texas at Austin
Los Alamos National Lab
Texas A&M University
University of Hawaii

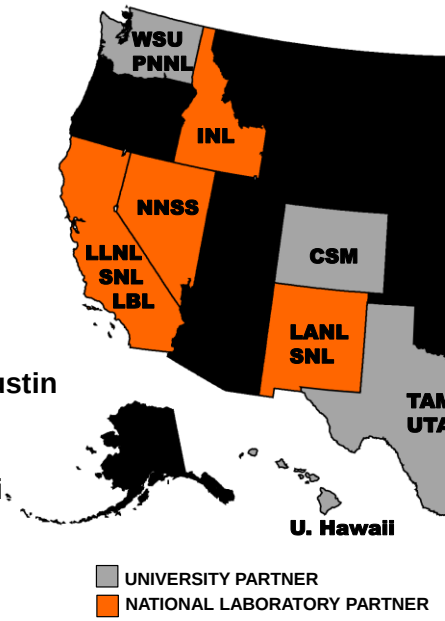

Massachusetts Institute of Technology
University of Wisconsin
The Ohio State University
University of Michigan
Argonne National Lab
Brookhaven National Lab
Princeton Plasma Physics Lab
University of North Carolina
Duke University
Savannah River National Lab
Oak Ridge National Lab
Claflin University
Georgia Institute of Technology
Spelman College

Univ. logo